Power-Efficient and Secure WPCNs With Hardware Impairments and Non-Linear EH Circuit

Elena Boshkovska, *Student Member, IEEE*, Derrick Wing Kwan Ng, *Senior Member, IEEE*, Linglong Dai, *Senior Member, IEEE*, and Robert Schober, *Fellow, IEEE*

***Abstract*— In this paper, we design a robust resource allocation algorithm for a wireless-powered communication network (WPCN) taking into account residual hardware impairments (HWIs) at the transceivers, the imperfectness of the channel state information, and the non-linearity of practical radio frequency energy harvesting circuits. In order to ensure power-efficient secure communication, physical layer security techniques are exploited to deliberately degrade the channel quality of a multiple-antenna eavesdropper. The resource allocation algorithm design is formulated as a non-convex optimization problem for minimization of the total power consumption in the network, while guaranteeing the quality of service of the information receivers in terms of secrecy rate. The globally optimal solution of the optimization problem is obtained via a 2-D search and semidefinite programming relaxation. To strike a balance between computational complexity and system performance, a low-complexity iterative suboptimal resource allocation algorithm is also proposed. Numerical results demonstrate that both the proposed optimal and suboptimal schemes can significantly reduce the total system power consumption required for guaranteeing secure communication, and unveil the impact of HWIs on the system performance: 1) residual HWIs create a system performance bottleneck in WPCN in the high transmit/receive power regimes; 2) increasing the number of transmit antennas can effectively reduce the power consumption of wireless power transfer and alleviate the performance degradation due to residual HWIs; and 3) imperfect CSI exacerbates the impact of residual HWIs, which increases the power consumption of both wireless power and wireless information transfer.**

***Index Terms*— Hardware impairments, wireless-powered communication, non-linear energy harvesting model, energy beamforming, physical layer security.**

Manuscript received September 13, 2017; revised November 20, 2017; accepted December 5, 2017. Date of publication December 14, 2017; date of current version June 14, 2018. D. W. K. Ng is supported under Australian Research Council's Discovery Early Career Researcher Award funding scheme (DE170100137). L. Dai is supported by the National Natural Science Foundation of China for Outstanding Young Scholars (Grant No. 61722109). R. Schober is supported by the AvH Professorship Program of the Alexander von Humboldt Foundation. This paper was presented in part at the IEEE Globecom 2017 [1]. The associate editor coordinating the review of this paper and approving it for publication was Z. Zhang. *(Corresponding author: Derrick Wing Kwan Ng.)*

E. Boshkovska and R. Schober are with Friedrich-Alexander-Universität Erlangen-Nürnberg, 91054 Erlangen, Germany.

D. W. K. Ng is with the University of New South Wales, Sydney, NSW 2052, Australia (e-mail: w.k.ng@unsw.edu.au).

L. Dai is with the Tsinghua National Laboratory for Information Science and Technology, Tsinghua University, Beijing 100084, China.

Color versions of one or more of the figures in this paper are available online at http://ieeexplore.ieee.org.

Digital Object Identifier 10.1109/TCOMM.2017.2783628

I. Introduction

WIRELESS charging of battery-powered devices in wireless communication networks via wireless power transfer (WPT) technology could prolong the lifetime of the networks. In fact, the concept of wireless-powered communication networks (WPCNs), where wireless devices are powered via radio frequency (RF) electromagnetic waves, has gained considerable attention recently in the context of enabling sustainability via WPT [2]. In particular, it is expected that the number of interconnected wireless devices will increase to up to 50 billion by 2020 [3], due to the roll-out of the Internet-of-Things (IoT). A large portion of these wireless devices, some of which may be inaccessible for frequent battery replacement, could be powered wirelessly by dedicated power stations via RF-based WPT technology to facilitate their information transmissions [4]–[6]. Specifically, RF-based WPT offers a more stable and controllable source of energy compared to natural energy sources, such as solar, wind, and tidal, etc., which are usually climate and location dependent [7]–[9]. More importantly, RF-based WPT exploits the broadcast nature of the wireless medium which enables one-to-many simultaneous long-range wireless charging. On the other hand, the large number of wireless devices in future networks encourages the use of low-quality and low-cost hardware components in order to reduce deployment costs. However, RF transceivers equipped with cheap hardware components suffer from various kinds of hardware impairments (HWIs) resulting potentially in a performance degradation for communications. These HWIs are caused by non-linear power amplifiers, frequency and phase offsets, in-phase and quadrature (I/Q) imbalance, and quantization noise. Although the negative impact of HWIs on the system performance can be reduced by calibration and compensation algorithms, residual distortions at the transceivers that depend on the power of the transmitted/received signal are inevitable [10]–[15]. Hence, existing resource allocation algorithms for multiuser WPCNs, e.g. [4]–[6], designed based on the assumption of ideal hardware, may lead to substantial performance losses in practical systems.

The increasing number of wireless devices also poses a threat to communication security in future wireless networks due to the enormous amount of data transmitted over wireless channels [16]–[18]. Nowadays, wireless communication security is ensured by cryptographic encryption algorithms operating in the application layer. Unfortunately,

these traditional security methods may not be applicable in future wireless networks with large numbers of transceivers, since encryption algorithms usually require secure secret key distribution and management via an authenticated third party. Recently, physical layer (PHY) security has been proposed as an effective complementary technology to the existing encryption algorithms for providing secure communication [16]–[21]. Specifically, PHY security exploits the unique characteristics of wireless channels, such as fading, noise, and interference, to protect the communication between legitimate devices from eavesdropping. In this context, Wu *et al.* [18] designed a resource allocation algorithm that jointly optimizes the transmit power, the duration of WPT, and the direction of spatial beams to facilitate security in WPCNs. In [19], beamforming design was studied for secrecy provisioning in distributed antenna systems with WPT. Chen *et al.* [20] investigated the design of secure transmission in wireless-powered relaying systems. In [21], the use of a wireless-powered friendly jammer was proposed to enable secure communication in a point-to-point communication system. Niu *et al.* [22] proposed a suboptimal resource allocation algorithm for energy efficiency maximization in a secure multiple-input multiple-output (MIMO) simultaneous wireless information and power transfer (SWIPT) system taking into account the impact of non-linear energy harvesting circuits. Niu *et al.* [23] studied the joint design of a precoding matrix and power splitting ratios for maximization of the total harvested energy in a MIMO-SWIPT system. In [24], beamforming was designed to ensure communication security in SWIPT-based amplify-and-forward relaying networks. Bi and Chen [25] studied the secrecy outage probability of a wireless-powered communication system with a full-duplex jammer. In [26], the resource allocation was optimized to enable secure wireless powered communication networks employing an energy harvesting jammer. However, most of the existing works on secure WPT systems are based on the assumption of ideal hardware [18]–[26] and are not applicable to practical systems suffering from HWIs. Recently, the notion of secure communication under the consideration of HWIs has been pursued. For instance, the work in [27] considered the analysis and design of secure massive MIMO systems in the presence of a passive eavesdropper and HWIs at the transceivers. Besides, Nguyen *et al.* [28] studied the impact of residual HWIs on the performance of a two-way WPT-based cognitive relay network, where the relay is powered by harvesting energy from the signals transmitted by the source in the RF. Zhu *et al.* [29] analyzed the impact of phase noise on downlink WPT in secure multiple antennas systems. However, Nguyen and Matthaiou [28] and Zhu *et al.* [29] assumed an overly simplified linear energy harvesting (EH) model for the end-to-end WPT characteristic. Yet, measurements of practical RF-based EH circuits demonstrate a highly non-linear end-to-end WPT characteristic [30], which implies that transmission schemes and algorithms designed based on the conventional linear EH model may cause performance degradation in practical implementations. Moreover, the transmission strategies in [27]–[29] were not optimized. Hence, the design of resource allocation for secure communication in WPCNs with the non-linear EH circuits suffering from HWIs is an important open problem.

To address the above issues, we propose a resource allocation algorithm design, which aims at providing power-efficient and secure communication in WPCNs in the presence of a multiple-antenna eavesdropper. The resource allocation algorithm design is formulated as a non-convex optimization problem taking into account the non-linearity of the EH circuits, the existence of residual HWIs at the transceivers, and the imperfectness of the channel state information (CSI) of the eavesdropper. We minimize the total consumed power while guaranteeing the quality of service (QoS) at the information receivers (IRs) in the WPCN. In general, there is no standard approach for solving non-convex optimization problems. In the extreme case, an exhaustive search with respect to all optimization variables is needed to obtain the global optimal solution which is computationally infeasible for a moderate problem size. Nevertheless, by exploiting the particular structure of the problem at hand, the optimal solution of the proposed problem is obtained via a two-dimensional search and semidefinite programming (SDP) relaxation. The proposed solution unveils that information beamforming from the access point in the direction of the IRs is optimal and that the SDP relaxation is tight. In addition, an iterative suboptimal scheme is proposed to reduce computational complexity. Numerical results demonstrate that the proposed schemes can significantly reduce the power consumption in the considered WPCN compared to two baseline schemes.

The remainder of this paper is organized as follows. In Section II, we introduce the adopted WPCN, HWI, and non-linear energy harvesting models. In Section III, we formulate the resource allocation algorithm design as a non-convex optimization problem, which is solved by an iterative resource allocation algorithm in Section IV. Section V presents simulation results for the system performance, and in Section VI, we conclude with a brief summary of our results.

II. System Model

In this section, we first present some notations and the considered system model. Then, we discuss the energy harvesting and hardware impairment models adopted for power-efficient resource allocation algorithm design.

A. Notation

We use boldface capital and lower case letters to denote matrices and vectors, respectively. $\mathbf{A}^H$, $\mathrm{Tr}(\mathbf{A})$, $\det(\mathbf{A})$, $\mathbf{A}^{-1}$, $\mathrm{Rank}(\mathbf{A})$, and $\lambda_{\max}(\mathbf{A})$ represent the Hermitian transpose, trace, determinant, inverse, rank, and maximum eigenvalue of matrix $\mathbf{A}$, respectively; $\mathbf{A} \succeq \mathbf{0}$ indicates that $\mathbf{A}$ is a positive semidefinite matrix; $\mathbf{I}_N$ denotes the $N \times N$ identity matrix. $\mathbb{C}^{N\times M}$ denotes the space of all $N \times M$ matrices with complex entries. $\mathbb{H}^N$ represents the set of all N-by-N complex Hermitian matrices. $|\cdot|$ and $\|\cdot\|_{\mathrm{F}}$ represent the absolute value of a complex scalar and the Frobenius norm, respectively. The distribution of a circularly symmetric complex Gaussian (CSCG) vector with mean vector $\mathbf{x}$ and covariance matrix $\mathbf{\Sigma}$ is denoted by $\mathcal{CN}(\mathbf{x}, \mathbf{\Sigma})$, and $\sim$ means "distributed as". $\mathcal{E}\{\cdot\}$ denotes

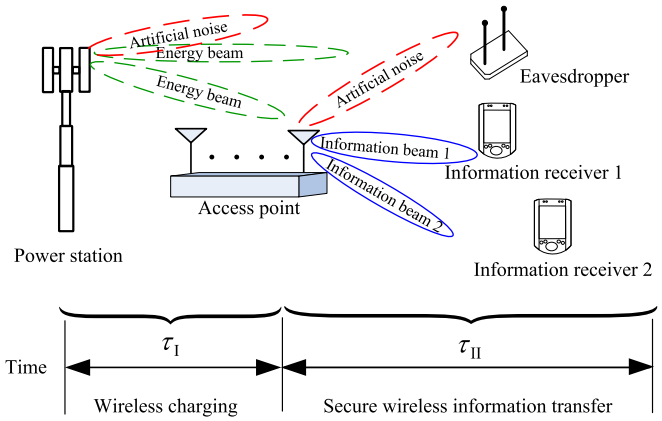

Fig. 1. A WPCN employing two transmission phases with $K = 2$ information receivers (IRs) and one multiple-antenna eavesdropper.

statistical expectation. $[x]^+$ stands for $\max\{0, x\}$. $\nabla_{\mathbf{x}} f(\mathbf{x})$ represents the partial derivative of function $f(\mathbf{x})$ with respect to the elements of vector $\mathbf{x}$. Furthermore, diag[$\mathbf{x}$] is a diagonal matrix with the elements of $\mathbf{x}$ on the main diagonal. $[\mathbf{A}]_{n,n}$ returns the element in the n-th row and n-th column of square matrix $\mathbf{A}$. $\mathbf{S}_m$ is a square matrix with all entries equal to 0 except for the m-th diagonal element which is equal to 1.

B. System Model

We focus on a WPCN which consists of a power station[1] (PS), an access point (AP), K IRs, and one eavesdropper (Eve), cf. Figure 1. We assume that the PS, the AP, and Eve are equipped with $N_{\mathrm{PS}} \geq 1$, $N_{\mathrm{AP}} \geq 1$, and $N_{\mathrm{EV}} \geq 1$ antennas,[2] respectively. The IRs are single-antenna devices for hardware simplicity. The communication in the WPCN comprises two transmission phases as shown in Figure 1. We assume that the fading channels in both phases are frequency flat and slowly time-varying. In particular, Phase I, with a time duration of τ_{I}, is reserved for wireless charging, where the PS transmits a dedicated energy beam to the energy-constrained AP. The instantaneous received signal at the AP during Phase I is given by

$$\mathbf{y}_{\mathrm{AP}} = \mathbf{L}^H\left(\mathbf{v} + \boldsymbol{\xi}^{(t)}\right) + \boldsymbol{\xi}^{(r)} + \mathbf{n}_{\mathrm{AP}}, \tag{1}$$

where $\mathbf{v} \in \mathbb{C}^{N_{\mathrm{PS}}\times 1}$ is the energy signal vector adopted in Phase I for wireless charging with covariance matrix $\mathbf{V} = \mathcal{E}\{\mathbf{v}\mathbf{v}^H\}$. The channel matrix between the PS and the AP is denoted by $\mathbf{L} \in \mathbb{C}^{N_{\mathrm{PS}}\times N_{\mathrm{AP}}}$ and captures the joint effect of path loss and multipath fading. Vector $\mathbf{n}_{\mathrm{AP}} \sim \mathcal{CN}(\mathbf{0}, \sigma_n^2\mathbf{I}_{N_{\mathrm{AP}}})$ represents the additive white Gaussian noise (AWGN) at the AP where σ_n^2 denotes the noise variance at each antenna of the AP. In (1), $\boldsymbol{\xi}^{(t)} \in \mathbb{C}^{N_{\mathrm{PS}}\times 1}$ and $\boldsymbol{\xi}^{(r)} \in \mathbb{C}^{N_{\mathrm{AP}}\times 1}$ represent the random residual HWIs after compensation introduced at the transmitter and receiver during Phase I, respectively. The model adopted for the residual HWIs will be presented later in the next section.

In Phase II, for a time duration of τ_{II}, the AP transmits K independent signals to the K IRs simultaneously. Because of the broadcast nature of wireless channels, there is a security threat due to potential eavesdropping. To circumvent this threat, both the AP and the PS deliberately emit artificial noise to degrade the channel quality of the eavesdropper [16]. Therefore, the instantaneous received signal at IR k in Phase II is given by

$$y_{\mathrm{IR}_k} = \mathbf{h}_k^H\Bigg(\sum_{i=1}^{K}\mathbf{w}_i s_i + \underbrace{\mathbf{u}}_{\text{Jamming from AP}} + \boldsymbol{\varsigma}^{(t)}\Bigg) + \mathbf{f}_k^H\Bigg(\underbrace{\mathbf{z}}_{\text{Jamming from PS}} + \boldsymbol{\kappa}^{(t)}\Bigg) + \varsigma_k^{(r)} + n_{\mathrm{IR}_k}, \tag{2}$$

where $s_k \in \mathbb{C}$ and $\mathbf{w}_k \in \mathbb{C}^{N_{\mathrm{AP}}\times 1}$ are the information symbol for IR k and the corresponding beamforming vector, respectively. Without loss of generality, we assume that $\mathcal{E}\{|s_k|^2\} = 1, \forall k$. $\mathbf{h}_k \in \mathbb{C}^{N_{\mathrm{AP}}\times 1}$ is the channel vector between the AP and IR k, while $\mathbf{f}_k \in \mathbb{C}^{N_{\mathrm{PS}}\times 1}$ denotes the channel vector between the PS and IR k. Furthermore, $\mathbf{u} \sim \mathcal{CN}(\mathbf{0}, \mathbf{U})$ and $\mathbf{z} \sim \mathcal{CN}(\mathbf{0}, \mathbf{Z})$ are the Gaussian pseudo-random energy signal sequences, i.e., the artificial noise, broadcasted by the AP and the PS, respectively, where $\mathbf{U} \in \mathbb{H}^{N_{\mathrm{AP}}}, \mathbf{U} \succeq \mathbf{0}$, and $\mathbf{Z} \in \mathbb{H}^{N_{\mathrm{PS}}}, \mathbf{Z} \succeq \mathbf{0}$, denote the corresponding covariance matrices, respectively. These two noise processes are exploited by the AP and the PS to degrade the channel quality of the eavesdropper via jamming. $\boldsymbol{\varsigma}^{(t)} \in \mathbb{C}^{N_{\mathrm{AP}}\times 1}$ and $\boldsymbol{\kappa}^{(t)} \in \mathbb{C}^{N_{\mathrm{PS}}\times 1}$ represent the random residual transmitter HWIs after compensation introduced by the AP and the PS in Phase II, respectively, while $\varsigma_k^{(r)} \in \mathbb{C}$ represents the residual receiver HWIs introduced by IR k. $n_{\mathrm{IR}_k} \sim \mathcal{CN}(0, \sigma_{\mathrm{IR}_k}^2)$ is the AWGN at IR k with noise power $\sigma_{\mathrm{IR}_k}^2$.

The instantaneous received signal at Eve in Phase II is given by

$$\mathbf{y}_{\mathrm{E}} = \mathbf{G}^H\Bigg(\sum_{i=1}^{K}\mathbf{w}_i s_i + \underbrace{\mathbf{u}}_{\text{Jamming from AP}} + \boldsymbol{\varsigma}^{(t)}\Bigg) + \mathbf{E}^H\Bigg(\underbrace{\mathbf{z}}_{\text{Jamming from PS}} + \boldsymbol{\kappa}^{(t)}\Bigg) + \mathbf{n}_{\mathrm{E}}, \tag{3}$$

where $\mathbf{G} \in \mathbb{C}^{N_{\mathrm{AP}}\times N_{\mathrm{E}}}$ and $\mathbf{E} \in \mathbb{C}^{N_{\mathrm{PS}}\times N_{\mathrm{E}}}$ denote the channel matrices of the AP-to-Eve links and the PS-to-Eve links, respectively. $\mathbf{n}_{\mathrm{E}} \sim \mathcal{CN}(\mathbf{0}, \sigma_{\mathrm{E}}^2\mathbf{I}_{N_{\mathrm{EV}}})$ is the AWGN vector at the eavesdropper with noise power σ_{E}^2. In this work, we assume that ideal hardware is available at the eavesdropper, i.e., there are no HWIs at the eavesdropper, which constitutes the worst case for communication security.

C. Hardware Impairment Model

In this paper, we adopt the general HWI model proposed in [15, Ch. 4] and [31, Ch. 7]. In particular, the residual distortion caused by the aggregate effect of different HWIs, such as I/Q imbalance, phase noise, and power amplifier non-linearities is modeled as a Gaussian random variable whose variance scales

[1] In this work, we assume that the PS is connected to the main grid with a continuous and stable energy supply.

[2] We note that an eavesdropper equipped with N_{EV} antennas is equivalent to multiple cooperating eavesdroppers with a total of N_{EV} antennas which are connected to a joint processing unit. Besides, we assume $N_{\mathrm{PS}} + N_{\mathrm{AP}} \geq N_{\mathrm{EV}}$ to enable secure communication.

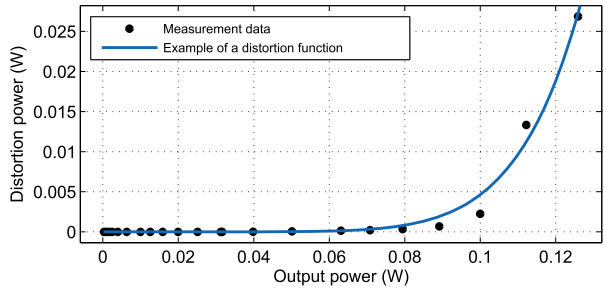

Fig. 2. A comparison between the convex distortion model in (6) and measurement data for a long term evolution (LTE) transmitter power amplifier [32]. In this example, parameters $k_1 = 2.258 \times 10^5$ and $k_2 = 7.687$ in (6) are calculated by a standard curve fitting tool.

with the power of the signals transmitted and received by the transmitter and the receiver, respectively. This model has been widely used in the literature to study the impact of transceiver HWIs on the performance of communication systems [11], [13], [28]. Besides, Studer *et al.* [13] showed that this model accurately captures the residual distortions caused by the joint effect of various HWIs in practical multiple-antenna systems.

Hence, the distortion noises caused by the transmitter HWIs at the PS in Phase I and Phase II are modeled as $\boldsymbol{\xi}^{(t)} \sim \mathcal{CN}(\mathbf{0}, \boldsymbol{\Phi})$ and $\boldsymbol{\kappa}^{(t)} \sim \mathcal{CN}(\mathbf{0}, \boldsymbol{\Theta})$, respectively. $\boldsymbol{\Phi} \in \mathbb{C}^{N_{\mathrm{PS}} \times N_{\mathrm{PS}}}$ and $\boldsymbol{\Theta} \in \mathbb{C}^{N_{\mathrm{PS}} \times N_{\mathrm{PS}}}$ are diagonal covariance matrices which contain on their main diagonal the distortion noise variances of each antenna of the PS in Phase I and Phase II, respectively, and are given by

$$\boldsymbol{\Phi} = \mathrm{diag}\left[\eta_1\left(P_{\mathrm{av},1}^{\mathrm{PS-I}}\right), \ldots, \eta_{N_{\mathrm{PS}}}\left(P_{\mathrm{av},N_{\mathrm{PS}}}^{\mathrm{PS-I}}\right)\right] \tag{4}$$

and

$$\boldsymbol{\Theta} = \mathrm{diag}\left[\eta_1\left(P_{\mathrm{av},1}^{\mathrm{PS-II}}\right), \ldots, \eta_{N_{\mathrm{PS}}}\left(P_{\mathrm{av},N_{\mathrm{PS}}}^{\mathrm{PS-II}}\right)\right]. \tag{5}$$

In (4) and (5), $P_{\mathrm{av},m}^{\mathrm{PS-I}} = \mathcal{E}\{\|\mathbf{S}_m\mathbf{v}\|_{\mathrm{F}}^2\} = [\mathbf{V}]_{m,m}$ and $P_{\mathrm{av},m}^{\mathrm{PS-II}} = \mathcal{E}\{\|\mathbf{S}_m\mathbf{z}\|_{\mathrm{F}}^2\} = [\mathbf{Z}]_{m,m}$, $m \in \{1, \ldots, N_{\mathrm{PS}}\}$, respectively, are the average powers of the transmit signal at the m-th antenna of the PS in Phase I and Phase II, respectively. Also, $\eta_m(\cdot), \forall m$, is a convex, continuous, and monotonically increasing distortion function which quantifies the impact of the HWIs for a given average power of the transmit signal at the m-th antenna,[3] i.e., the function maps the average power of the signal to a specific distortion value. For example, the transmitter distortion function can be modeled by the following convex increasing function:

$$\eta_m(x_m) = k_1 x_m^{k_2} \quad [\mathrm{Watt}], \tag{6}$$

where x_m [Watt] is the average transmit power at antenna m. Constants $k_1 \geq 0$ and $k_2 \geq 1$ are model parameters which are chosen such that they fit the measurements of the associated practical systems.[4] In Figure 2, we illustrate that the proposed model for the transmitter distortion function in (6) closely matches the experimental results in [32].

Similarly, the transmitter HWIs at the AP in Phase II are modeled as $\boldsymbol{\varsigma}^{(t)} \sim \mathcal{CN}(\mathbf{0}, \boldsymbol{\Psi})$ with covariance matrix

$$\boldsymbol{\Psi} = \mathrm{diag}\left[\eta_1\left(P_{\mathrm{av},1}^{\mathrm{AP}}\right), \ldots, \eta_{N_{\mathrm{AP}}}\left(P_{\mathrm{av},N_{\mathrm{AP}}}^{\mathrm{AP}}\right)\right], \tag{7}$$

where $P_{\mathrm{av},n}^{\mathrm{AP}} = \mathcal{E}\left\{\|\mathbf{S}_n(\sum_{k=1}^K \mathbf{w}_k s_k + \mathbf{u})\|_{\mathrm{F}}^2\right\} = \left[\sum_{k=1}^K \mathbf{w}_k\mathbf{w}_k^H + \mathbf{U}\right]_{n,n}$, $\forall n \in \{1, \ldots, N_{\mathrm{AP}}\}$. On the other hand, the received signal is affected mostly by phase noises and I/Q imbalances [31, Ch. 7]. In the considered WPCN, these residual HWIs are modeled by the receiver distortion noise at the AP, $\boldsymbol{\xi}^{(r)} \in \mathbb{C}^{N_{\mathrm{AP}} \times 1}$, cf. (1), where $\boldsymbol{\xi}^{(r)} \sim \mathcal{CN}(\mathbf{0}, \sigma_{d_{\mathrm{AP}}}^2\mathbf{I}_{N_{\mathrm{AP}}})$. Moreover, $\sigma_{d_{\mathrm{AP}}}^2 = \nu\left(\mathcal{E}\{\|\mathbf{L}^H\mathbf{v}\|_{\mathrm{F}}^2\}\right) = \nu\left(\mathrm{Tr}(\mathbf{V}\mathbf{L}\mathbf{L}^H)\right)$, where $\nu(\cdot)$ is a convex, continuous, and monotonically increasing function that models the receiver impairment characteristic. Additionally, the receiver HWIs at each IR during Phase II are given by $\varsigma_k^{(r)} \sim \mathcal{CN}(0, \sigma_{d_{\mathrm{IR}_k}}^2)$, with $\sigma_{d_{\mathrm{IR}_k}}^2 = \nu\left(\mathcal{E}\{\|\mathbf{h}_k^H(\sum_{i=1}^K \mathbf{w}_i s_i + \mathbf{u}) + \mathbf{f}_k^H\mathbf{z}\|_{\mathrm{F}}^2\}\right) = \nu\left(\mathrm{Tr}(\mathbf{H}_k(\mathbf{U} + \sum_{i=1}^K \mathbf{w}_i\mathbf{w}_i^H) + \mathbf{F}_k\mathbf{Z})\right)$, where $\mathbf{F}_k = \mathbf{f}_k\mathbf{f}_k^H$ and $\mathbf{H}_k = \mathbf{h}_k\mathbf{h}_k^H$ are introduced for notational simplicity. According to [11], a suitable choice of the receiver distortion function is $\nu(x) = (\frac{k_3}{100})^2 x$ [Watt], where x is the average power of the received signal and k_3 is a constant model parameter with a typical range of $k_3 \in [0, 15]$.

D. Energy Harvesting Model

In the considered WPCN, we exploit the energy and artificial noise signals transmitted by the PS in Phase I and Phase II to charge the AP and to facilitate secure information transfer, respectively. In this paper, we adopt the practical non-linear RF-based EH model proposed in [33] to characterize the end-to-end WPT at the AP. The total energy harvested by the AP in Phase I is given by

$$\Xi_{\mathrm{tot}}(\omega) = \frac{\frac{M}{1+\exp(-a(\omega-b))} - M\Omega}{1-\Omega}, \quad \Omega = \frac{1}{1+\exp(ab)},$$
$$\omega = \mathrm{Tr}\left(\mathbf{L}^H(\mathbf{V} + \boldsymbol{\Phi})\mathbf{L}\right), \tag{8}$$

where ω represents the received RF power at the AP. The parameters M, a, and b in (8) capture the joint effects of various non-linear phenomena caused by hardware limitations in practical EH circuits. More specifically, M represents the maximum power that can be harvested by the EH circuit, as the circuit becomes saturated for exceedingly large received RF powers. Moreover, a and b depend on several physical hardware phenomena, such as circuit sensitivity and potential current leakage. In fact, the adopted non-linear EH model was shown to accurately characterize the behavior of various practical EH circuits [33]–[35]. In contrast, the conventional linear EH model, which is widely used in the literature [18]–[21], [28], may lead to performance degradation due to a severe model mismatch for resource allocation algorithm design.

[3]Note that the model considered here directly maps the signal power to the distortion power while the one proposed in [15, Ch. 4] maps the signal magnitude to the distortion magnitude.

[4]In practice, the value of the distortion function of the transmitter HWIs usually grows at least linearly with respect to the transmit power which leads to $k_2 \geq 1$.

Remark 1: In practice, the EH hardware circuit of the AP is fixed and parameters a, b, and M of the non-linear model in (8) can be determined by a standard curve fitting tool.

E. Channel State Information

In practice, handshaking is performed between the legitimate PS, the AP, and the K IRs. As a result, accurate CSI can be obtained by exploiting the pilot sequences embedded in the handshaking signals. In this paper, we assume that the CSI of $\mathbf{L}$, $\mathbf{h}_k$, and $\mathbf{f}_k$ is available for resource allocation algorithm design. In contrast, the potential eavesdropper may not directly interact with the transmitters and it is difficult to obtain perfect CSI for the corresponding links. To capture the impact of imperfect CSI knowledge of the eavesdropper's channels on the system performance, we adopt the deterministic model from [34]–[38]. To this end, the CSI of the relevant communication links is modeled as

$$\mathbf{G} = \widehat{\mathbf{G}} + \Delta\mathbf{G},$$
$$\Xi_{\mathrm{E}}^{\mathrm{AP}} \triangleq \left\{\Delta\mathbf{G} \in \mathbb{C}^{N_{\mathrm{AP}}\times N_{\mathrm{E}}} : \|\Delta\mathbf{G}\|_{\mathrm{F}} \leq \upsilon_{\mathrm{AP}\to\mathrm{E}}\right\}, \quad (9)$$
$$\mathbf{E} = \widehat{\mathbf{E}} + \Delta\mathbf{E},$$
$$\Xi_{\mathrm{E}}^{\mathrm{PS}} \triangleq \left\{\Delta\mathbf{E} \in \mathbb{C}^{N_{\mathrm{PS}}\times N_{\mathrm{E}}} : \|\Delta\mathbf{E}\|_{\mathrm{F}} \leq \upsilon_{\mathrm{PS}\to\mathrm{E}}\right\}, \quad (10)$$

respectively, where $\widehat{\mathbf{G}}$ and $\widehat{\mathbf{E}}$ are the estimates of channel matrices $\mathbf{G}$ and $\mathbf{E}$, respectively, for resource allocation. Matrices $\Delta\mathbf{G}$ and $\Delta\mathbf{E}$ represent the channel uncertainty which captures the joint effects of channel estimation errors and the time varying nature of the associated channels. In particular, the continuous sets $\Xi_{\mathrm{E}}^{\mathrm{AP}}$ and $\Xi_{\mathrm{E}}^{\mathrm{PS}}$ in (9) and (10), respectively, define the continuous spaces spanned by all possible channel uncertainties with respect to the associated channels. Constants $\upsilon_{\mathrm{AP}\to\mathrm{E}}$ and $\upsilon_{\mathrm{PS}\to\mathrm{E}}$, denote the maximum values of the norms of the CSI estimation error matrices $\Delta\mathbf{G}$ and $\Delta\mathbf{E}$, respectively. In practice, the values of $\upsilon_{\mathrm{AP}\to\mathrm{E}}$ and $\upsilon_{\mathrm{PS}\to\mathrm{E}}$ depend on the adopted channel estimation algorithms and the coherence times of the associated channels.

Remark 2: Although the eavesdropper may be passive and remain silent, its CSI can be estimated based on the power leakage of the local oscillator of its receiver RF front-end [39].

III. Resource Allocation Problem Formulation

In this section, we first define the system performance metrics and then we formulate the resource allocation algorithm design as an optimization problem.

A. Achievable Data Rate and Secrecy Rate

Given perfect CSI at the receiver, the achievable data rate of IR k in Phase II is given by

$$R_k = \tau_{\mathrm{II}} \log_2\left(1 + \Gamma_k\right), \text{ where} \quad (11)$$
$$\Gamma_k = \frac{\mathbf{w}_k^H \mathbf{H}_k \mathbf{w}_k}{\sum_{j\neq k} \mathbf{w}_j \mathbf{H}_k \mathbf{w}_j^H + I_k + \sigma_{d_{\mathrm{IR}_k}}^2 + \sigma_n^2} \quad (12)$$

and

$$I_k = \underbrace{\mathrm{Tr}(\mathbf{F}_k\boldsymbol{\Theta}) + \mathrm{Tr}(\boldsymbol{\Psi}\mathbf{H}_k)}_{\text{Interference due to transmitter HWIs}}. \quad (13)$$

Variable Γ_k is the received signal-to-interference-plus-noise ratio (SINR) at IR k. We note that since the pseudo-random artificial noise signals are known to all legitimate transceivers, the impact of the artificial noise signals on the desired signal can be removed at IR k via interference cancellation, i.e., $\mathrm{Tr}(\mathbf{H}_k\mathbf{U})$ and $\mathrm{Tr}(\mathbf{F}_k\mathbf{Z})$ have been removed[5] in (11).

On the other hand, as the computational capability of the eavesdropper is not known, we focus on the worst-case scenario for facilitating secrecy provisioning. In particular, we assume that the eavesdropper is equipped with a noiseless receiver and is able to remove all multiuser interference via successive interference cancellation before attempting to decode the information of IR k. As a result, the maximum rate at which the eavesdropper can decode the information intended for IR k is given by

$$C_k = \tau_{\mathrm{II}} \log_2 \det\left(\mathbf{I}_{N_{\mathrm{E}}} + \mathbf{Q}^{-1}\mathbf{G}^H\mathbf{w}_k\mathbf{w}_k^H\mathbf{G}\right), \quad (14)$$

where

$$\mathbf{Q} = \mathbf{G}^H\Big(\underbrace{\mathbf{U}}_{\text{Jamming from the AP}} + \boldsymbol{\Psi}\Big)\mathbf{G} + \mathbf{E}^H\Big(\underbrace{\mathbf{Z}}_{\text{Jamming from the PS}} + \boldsymbol{\Theta}\Big)\mathbf{E} \quad (15)$$

is the interference covariance matrix of the eavesdropper. The achievable secrecy rate between the AP and IR k is given by

$$R_k^{\mathrm{sec}} = \left[R_k - C_k\right]^+. \quad (16)$$

As can be seen from (14) and (16), in principle, both the artificial noise signals and the transmitter HWI signals can enhance communication secrecy by degrading the capacity of the channel of the eavesdropper.

B. Total Power Consumption

In this section, we study the power consumption in both transmission phases. Due to the residual HWIs at the transmitter of the PS, a portion of the transmitted power is wasted during Phase I. More specifically, the total power consumption in Phase I is given by

$$P_{\mathrm{PS-I}} = \rho_{\mathrm{PS}}\Big(\underbrace{\mathrm{Tr}(\mathbf{V})}_{\text{Power for charging}} + \underbrace{\mathrm{Tr}(\boldsymbol{\Phi})}_{\text{Power waste}}\Big) + P_{\mathrm{c_{PS}}}, \quad (17)$$

where $P_{\mathrm{c_{PS}}}$ accounts for the constant circuit power consumption at the PS. Besides, to capture the power inefficiency of practical power amplifiers, we introduce a linear multiplicative constant $\rho_{\mathrm{PS}} > 1$ for the power radiated by the PS [19], [40]. For example, if $\rho_{\mathrm{PS}} = 5$, then for every 1 Watt of power radiated in the RF, the PS consumes 5 Watt of power which leads to a power amplifier efficiency of 20%. In Phase II, the PS transmits artificial noise signals to degrade the channel quality of the eavesdropper and the associated power consumption is

$$P_{\mathrm{PS-II}} = \rho_{\mathrm{PS}}\Big(\underbrace{\mathrm{Tr}(\mathbf{Z})}_{\text{Power for jamming}} + \underbrace{\mathrm{Tr}(\boldsymbol{\Theta})}_{\text{Power waste}}\Big) + P_{\mathrm{c_{PS}}}. \quad (18)$$

[5]We note that the interference caused by the transmitter HWIs cannot be removed at IR k as it is an unknown random process.

On the other hand, in Phase II, the AP transmits K independent information signals to the K IRs concurrently. Besides, artificial noise is also emitted by the AP to degrade the channel quality of the eavesdropper. Because of the residual transmitter HWIs, a portion of the power is also wasted at the AP. Hence, the total power consumption at the AP is given by

$$P_{\mathrm{AP-II}} = \rho_{\mathrm{AP}}\Bigg(\underbrace{\sum_{k=1}^{K}\|\mathbf{w}_k\|^2}_{\text{Power for information transmission}} + \underbrace{\mathrm{Tr}(\mathbf{U})}_{\text{Power for jamming}} + \underbrace{\mathrm{Tr}(\mathbf{\Psi})}_{\text{Power waste}} \Bigg) + P_{\mathrm{c_{AP}}}. \tag{19}$$

Here, $P_{\mathrm{c_{AP}}}$ is the constant circuit power consumption and $\rho_{\mathrm{AP}} > 1$ denotes the power amplifier inefficiency at the AP.

C. Optimization Problem Formulation

In the following, we formulate an optimization problem for the minimization of the total power consumption in both transmission phases of the considered WPCN while guaranteeing secure communication in the presence of residual HWIs, imperfect CSI, and a non-linear EH model. The considered optimization problem is given by equation (20) at the bottom of this page. The objective function in (20) takes into account the total power consumption in Phases I and II at the PS and the AP,[6] cf. (17)–(19). Constraint C1 is imposed such that the achievable data rate of IR k in Phase II satisfies a minimum required data rate R_{req_k}. On the other hand, taking into account the impact of CSI imperfectness, i.e., sets $\mathbf{\Xi}_{\mathrm{E}}^{\mathrm{AP}}$ and $\mathbf{\Xi}_{\mathrm{E}}^{\mathrm{PS}}$, constant R_{tol} in C2 limits the maximum tolerable capacity achieved by Eve in attempting to decode the message of IR k. In practice, $R_{\mathrm{req}_k} \gg R_{\mathrm{tol}} > 0$ is set by the system operator to ensure secure communication.[7] $T_{\max}$ in constraint C3 specifies the total time available for both phases. C4 is a constraint on the overall energy consumption at the AP during Phase II. The total available energy at the AP comprises the energy harvested from the dedicated energy signal transmitted by the PS in Phase I and a constant energy $E_{\mathrm{res}} \geq 0$. In practice, E_{res} may represent the residual energy at the AP from previous transmissions or energy obtained from other sources. Furthermore, ϱ in C5 is an auxiliary optimization variable which represents the received RF power at the AP. In particular, C5 ensures that ϱ is always smaller or equal to the minimum harvested power. C6 is a non-negativity constraint on the durations of Phase I and Phase II, respectively. $P_{\max}^{\mathrm{PS}}$ in constraints C7 and C8 limits the maximum transmit power of the PS in Phase I and Phase II, respectively. Similarly, $P_{\max}^{\mathrm{AP}}$ in constraint C9 specifics the maximum transmit power allowance of the AP in Phase II. Constraint C10, $\mathbf{V} \in \mathbb{H}^{N_{\mathrm{PS}}}$, $\mathbf{Z} \in \mathbb{H}^{N_{\mathrm{PS}}}$, and $\mathbf{U} \in \mathbb{H}^{N_{\mathrm{AP}}}$ constrain matrices $\mathbf{V}$, $\mathbf{Z}$, and $\mathbf{U}$ to be positive semidefinite Hermitian matrices such that they are valid covariance matrices.

[6]The power consumptions are optimized in both phases, even though the AP is wirelessly charged by the PS only in Phase I. In fact, besides the energy harvested in Phase I, the AP can also use residual energy, E_{res}, remaining from previous transmission phases for transmission in the current Phase II, cf. constraint C4. Hence, the power consumption of Phase II should also be minimized as well.

[7]We note that the adopted problem formulation constraining the received SINR of the potential eavesdropper provides a higher flexibility for providing communication secrecy for different applications, e.g. video clips, images, etc., compared to a problem formulation which directly constrains the secrecy rate. Besides, the solution of (20) guarantees a minimum secrecy rate of $R_k^{\mathrm{sec}} = \left[R_{\mathrm{req}_k} - R_{\mathrm{tol}}\right]^+$ for IR k.

[8]For resource allocation algorithm design, we assume that the problem in (20) is feasible. We note that the feasibility of (20) can be ensured by a suitable scheduling of the IRs in the media access control layer.

IV. Resource Allocation Algorithm Design

The resource allocation problem in (20) is a non-convex optimization problem. In fact, the right-hand side of constraint C4 is a quasi-concave function with respect to τ_{I} and ϱ. Besides, the optimization variables are coupled in the objective function and in constraint C4. Also, constraint C2 involves infinitely many possibilities due to the uncertainties of the channel estimation errors. Furthermore, the log-det function in constraint C2 is generally intractable. In this section, we first study the design of a globally optimal resource allocation scheme.[8] The performance of this scheme serves as a

$$\begin{aligned}
&\underset{\substack{\tau_{\mathrm{I}},\tau_{\mathrm{II}},\varrho,\mathbf{V}\in\mathbb{H}^{N_{\mathrm{PS}}},\mathbf{Z}\in\mathbb{H}^{N_{\mathrm{PS}}},\\ \mathbf{U}\in\mathbb{H}^{N_{\mathrm{AP}}},\mathbf{w}_k}}{\text{minimize}} \quad \tau_{\mathrm{I}} P_{\mathrm{PS-I}} + \tau_{\mathrm{II}}\Big(P_{\mathrm{AP-II}} + P_{\mathrm{PS-II}}\Big)\\
&\text{s.t. C1:}\ \ \tau_{\mathrm{II}}\log_2\left(1+\Gamma_k\right) \geq R_{\mathrm{req}_k}, \quad \forall k,\\
&\quad \text{C2:}\ \ \max_{\Delta\mathbf{G}\in\mathbf{\Xi}_{\mathrm{E}}^{\mathrm{AP}},\Delta\mathbf{E}\in\mathbf{\Xi}_{\mathrm{E}}^{\mathrm{PS}}} \tau_{\mathrm{II}}\log_2\det\left(\mathbf{I}_{N_{\mathrm{E}}} + \mathbf{Q}^{-1}\mathbf{G}^H\mathbf{w}_k\mathbf{w}_k^H\mathbf{G}\right) \leq R_{\mathrm{tol}}, \quad \forall k,\\
&\quad \text{C3:}\ \ \tau_{\mathrm{I}} + \tau_{\mathrm{II}} \leq T_{\max},\\
&\quad \text{C4:}\ \ \tau_{\mathrm{II}}\left(P_{\mathrm{c_{AP}}} + \rho_{\mathrm{AP}}\left(\sum_{k=1}^{K}\|\mathbf{w}_k\|^2 + \mathrm{Tr}(\mathbf{U}) + \mathrm{Tr}(\mathbf{\Psi})\right)\right) \leq \tau_{\mathrm{I}}\Xi_{\mathrm{tot}}(\varrho) + E_{\mathrm{res}},\\
&\quad \text{C5:}\ \ \varrho \leq \mathrm{Tr}(\mathbf{L}^H(\mathbf{V}+\mathbf{\Phi})\mathbf{L}), \quad \text{C6:}\ \ \tau_{\mathrm{I}},\tau_{\mathrm{II}} \geq 0,\\
&\quad \text{C7:}\ \ \mathrm{Tr}(\mathbf{V}) + \mathrm{Tr}(\mathbf{\Phi}) \leq P_{\max}^{\mathrm{PS}}, \quad \text{C8:}\ \ \mathrm{Tr}(\mathbf{Z}) + \mathrm{Tr}(\mathbf{\Theta}) \leq P_{\max}^{\mathrm{PS}},\\
&\quad \text{C9:}\ \ \sum_{k=1}^{K}\|\mathbf{w}_k\|^2 + \mathrm{Tr}(\mathbf{U}) + \mathrm{Tr}(\mathbf{\Psi}) \leq P_{\max}^{\mathrm{AP}}, \quad \text{C10:}\ \ \mathbf{Z},\mathbf{V},\mathbf{U} \succeq \mathbf{0}.
\end{aligned} \tag{20}$$

performance upper bound for any suboptimal scheme. Then, we derive a computationally efficient suboptimal resource allocation algorithm.

A. Optimal Resource Allocation

To obtain a globally optimal resource allocation scheme, we first perform the following transformation steps. In particular, we introduce auxiliary optimization matrices, $\mathbf{B}_{\mathrm{PS-I}} \in \mathbb{C}^{N_{\mathrm{PS}} \times N_{\mathrm{PS}}}$, $\mathbf{B}_{\mathrm{PS-II}} \in \mathbb{C}^{N_{\mathrm{PS}} \times N_{\mathrm{PS}}}$, and $\mathbf{B}_{\mathrm{AP}} \in \mathbb{C}^{N_{\mathrm{AP}} \times N_{\mathrm{AP}}}$, which account for the HWIs at the PS and the AP, respectively. Additionally, we introduce auxiliary optimization variables, $r_{\mathrm{IR},k}, \forall k$, which represent the distortion noise terms caused by the receiver HWIs at the IRs. Then, we transform problem (20) into the equivalent rank-constrained SDP optimization problem[9] with optimization variable set $\mathcal{P} = \{\varrho, \mathbf{V} \in \mathbb{C}^{N_{\mathrm{PS}}}, \mathbf{Z} \in \mathbb{C}^{N_{\mathrm{PS}}}, \mathbf{U} \in \mathbb{C}^{N_{\mathrm{AP}}}, \mathbf{B}_{\mathrm{PS-I}}, \mathbf{B}_{\mathrm{PS-II}}, \mathbf{B}_{\mathrm{AP}}, r_{\mathrm{IR},k}\}$ given by equation (21) at the bottom of this page, where $\Gamma_{\mathrm{req}_k} = 2^{R_{\mathrm{req}_k}/\tau_{\mathrm{II}}} - 1, \forall k$, and $\Gamma_{\mathrm{tol}} = 2^{R_{\mathrm{tol}}/\tau_{\mathrm{II}}} - 1$ are the equivalent required and maximum tolerable SINRs at IR k and the eavesdropper, respectively. The power consumption in Phase I and Phase II in the objective function can be rewritten as

$$\widetilde{P}_{\mathrm{PS-I}} = \rho_{\mathrm{PS}}\left(\mathrm{Tr}(\mathbf{V}) + \sum_{m=1}^{N_{\mathrm{PS}}} \mathrm{Tr}(\mathbf{S}_m \mathbf{B}_{\mathrm{PS-I}})\right) + P_{\mathrm{c_{PS}}}, \tag{22}$$

$$\widetilde{P}_{\mathrm{PS-II}} = \rho_{\mathrm{PS}}\left(\mathrm{Tr}(\mathbf{Z}) + \sum_{m=1}^{N_{\mathrm{PS}}} \mathrm{Tr}(\mathbf{S}_m \mathbf{B}_{\mathrm{PS-II}})\right) + P_{\mathrm{c_{PS}}}, \tag{23}$$

[9]In this paper, equivalent means that the transformed problem and the original problem share the same optimal solution.

$$\widetilde{P}_{\mathrm{AP-II}} = \rho_{\mathrm{AP}}\left(\sum_{k=1}^{K} \mathrm{Tr}(\mathbf{w}_k \mathbf{w}_k^H) + \mathrm{Tr}(\mathbf{U}) + \sum_{n=1}^{N_{\mathrm{AP}}} \mathrm{Tr}(\mathbf{S}_n \mathbf{B}_{\mathrm{AP}})\right) + P_{\mathrm{c_{AP}}}. \tag{24}$$

Furthermore, constraint C2 in (20) is replaced by constraint $\widetilde{\mathrm{C2}}$ in (21). These two constraints are equivalent when $R_{\mathrm{tol}} > 0$ and $\mathrm{Rank}(\mathbf{w}_k \mathbf{w}_k^H) \leq 1$, cf. [36]. Constraints $\widetilde{\mathrm{C4}}$, $\widetilde{\mathrm{C5}}$, and $\widetilde{\mathrm{C7}} - \widetilde{\mathrm{C9}}$ are equivalent to the original constraints C4, C5, and C7−C9, respectively, as the new convex constraints C12−C15 are satisfied with equality at the optimal solution.

Next, we handle the coupling of the optimization variables in the objective function and constraint $\widetilde{\mathrm{C4}}$. When both τ_{I} and τ_{II} are fixed, we can solve (21) for the remaining optimization variables. In fact, for a fixed τ_{I}, the quasi-concavity of the right-hand side of constraint $\widetilde{\mathrm{C4}}$ is also resolved. Besides, the right-hand side of constraint $\widetilde{\mathrm{C4}}$ is concave with respect to ϱ. As a result, we study the optimal resource allocation by assuming that the optimal values of τ_{I} and τ_{II} satisfying constraints C3 and C6 are found by a two-dimensional grid search.

Hence, we recast the original problem as an equivalent rank-constrained SDP optimization problem. To this end, we define $\mathbf{W}_k = \mathbf{w}_k \mathbf{w}_k^H$ and rewrite the problem in (21) as equation (25) at the top of next page, where $\mathbf{\Lambda} = \{a_n, b_m, c_d, d_k, \forall k\}$ is a set of auxiliary optimization variables. We note that the new sets of constraint pairs {C12a, C12b}, {C13a, C13b}, {C14a, C14b}, and {C15a, C15b} are equivalent to the original constraints C12, C13, C14, and C15, respectively, as the new constraint pairs are satisfied with equality for the optimal solution. Besides, constraints C16 and C17 are imposed to guarantee that $\mathbf{W}_k = \mathbf{w}_k \mathbf{w}_k^H$ holds for the optimal solution.

$$\begin{aligned}
&\underset{\tau_{\mathrm{I}}, \tau_{\mathrm{II}}, \mathcal{P}, \mathbf{w}_k}{\text{minimize}} \quad \tau_{\mathrm{I}} \widetilde{P}_{\mathrm{PS-I}} + \tau_{\mathrm{II}} (\widetilde{P}_{\mathrm{AP-II}} + \widetilde{P}_{\mathrm{PS-II}}) \\
&\text{s.t. } \widetilde{\mathrm{C1}}\text{:} \ \frac{\mathbf{w}_k^H \mathbf{H}_k \mathbf{w}_k}{\Gamma_{\mathrm{req}_k}} \geq \sum_{j \neq k} \mathbf{w}_j^H \mathbf{H}_k \mathbf{w}_j + \sum_{n=1}^{N_{\mathrm{AP}}} \mathrm{Tr}(\mathbf{S}_n \mathbf{B}_{\mathrm{AP}} \mathbf{H}_k) + \sum_{n=1}^{N_{\mathrm{PS}}} \mathrm{Tr}(\mathbf{S}_n \mathbf{B}_{\mathrm{PS-II}} \mathbf{F}_k) + r_{\mathrm{IR},k} + \sigma_n^2, \quad \forall k, \\
&\quad \widetilde{\mathrm{C2}}\text{:} \ \max_{\Delta \mathbf{G} \in \Xi_{\mathrm{E}}^{\mathrm{AP}}, \Delta \mathbf{E} \in \Xi_{\mathrm{E}}^{\mathrm{PS}}} \frac{\mathbf{G}^H \mathbf{w}_k \mathbf{w}_k^H \mathbf{G}}{\Gamma_{\mathrm{tol}}} \preceq \mathbf{G}^H (\mathbf{U} + \mathbf{B}_{\mathrm{PS}}) \mathbf{G} + \mathbf{E}^H (\mathbf{Z} + \mathbf{B}_{\mathrm{PS-II}}) \mathbf{E}, \quad \forall k, \\
&\quad \widetilde{\mathrm{C4}}\text{:} \ \tau_{\mathrm{II}} \widetilde{P}_{\mathrm{AP-II}} \leq \tau_{\mathrm{I}} \Xi_{\mathrm{tot}}(\varrho) + E_{\mathrm{res}}, \quad \mathrm{C3}, \ \mathrm{C6}, \ \mathrm{C10}, \\
&\quad \widetilde{\mathrm{C5}}\text{:} \ \varrho \leq \mathrm{Tr}(\mathbf{L}^H (\mathbf{V} + \mathbf{B}_{\mathrm{PS-I}}) \mathbf{L}), \\
&\quad \widetilde{\mathrm{C7}}\text{:} \ \mathrm{Tr}(\mathbf{V}) + \sum_{m=1}^{N_{\mathrm{PS}}} \mathrm{Tr}(\mathbf{S}_m \mathbf{B}_{\mathrm{PS-I}}) \leq P_{\max}^{\mathrm{PS}}, \quad \widetilde{\mathrm{C8}}\text{:} \ \mathrm{Tr}(\mathbf{Z}) + \sum_{m=1}^{N_{\mathrm{PS}}} \mathrm{Tr}(\mathbf{S}_m \mathbf{B}_{\mathrm{PS-II}}) \leq P_{\max}^{\mathrm{PS}}, \\
&\quad \widetilde{\mathrm{C9}}\text{:} \ \sum_{k=1}^{K} \|\mathbf{w}_k\|^2 + \mathrm{Tr}(\mathbf{U}) + \sum_{n=1}^{N_{\mathrm{AP}}} \mathrm{Tr}(\mathbf{S}_n \mathbf{B}_{\mathrm{AP}}) \leq P_{\max}^{\mathrm{AP}}, \quad \mathrm{C11}\text{:} \ \mathbf{B}_{\mathrm{PS-I}}, \mathbf{B}_{\mathrm{PS-II}}, \mathbf{B}_{\mathrm{AP}} \succeq \mathbf{0}, \\
&\quad \mathrm{C12}\text{:} \ \eta_n \left(\sum_{k=1}^{K} [\mathbf{w}_k \mathbf{w}_k^H]_{n,n} + [\mathbf{U}]_{n,n}\right) \leq [\mathbf{B}_{\mathrm{AP}}]_{n,n}, \quad \forall n, \\
&\quad \mathrm{C13}\text{:} \ \eta_m \Big([\mathbf{V}]_{m,m}\Big) \leq [\mathbf{B}_{\mathrm{PS-I}}]_{m,m}, \quad \forall m, \quad \mathrm{C14}\text{:} \ \eta_m \Big([\mathbf{Z}]_{m,m}\Big) \leq [\mathbf{B}_{\mathrm{PS-II}}]_{m,m}, \quad \forall m, \\
&\quad \mathrm{C15}\text{:} \ \nu \left(\mathrm{Tr}(\mathbf{H}_k (\mathbf{U} + \sum_{i=1}^{K} \mathbf{w}_i \mathbf{w}_i^H) + \mathbf{F}_k \mathbf{Z})\right) \leq r_{\mathrm{IR},k}, \quad \forall k.
\end{aligned} \tag{21}$$

$$\begin{aligned}
&\underset{\varrho,\mathbf{W}_k\in\mathbb{H}^{N_{\mathrm{AP}}},\mathbf{\Lambda}}{\text{minimize}} \quad \tau_{\mathrm{I}}\widetilde{P}_{\mathrm{PS-I}}+\tau_{\mathrm{II}}(\widetilde{P}_{\mathrm{AP-II}}+\widetilde{P}_{\mathrm{PS-II}})\\
&\text{s.t. } \widetilde{\mathrm{C1}}\text{: } \frac{\mathrm{Tr}(\mathbf{H}_k\mathbf{W}_k)}{\Gamma_{\mathrm{req}_k}}\geq\sum_{j\neq k}\mathrm{Tr}(\mathbf{H}_k\mathbf{W}_j)+\sum_{n=1}^{N_{\mathrm{AP}}}\mathrm{Tr}(\mathbf{S}_n\mathbf{B}_{\mathrm{AP}}\mathbf{H}_k)+\sum_{n=1}^{N_{\mathrm{AP}}}\mathrm{Tr}(\mathbf{S}_n\mathbf{B}_{\mathrm{PS-II}}\mathbf{F}_k)+r_{\mathrm{IR},k}^2+\sigma_n^2,\quad\forall k,\\
&\widetilde{\mathrm{C2}}\text{: } \max_{\Delta\mathbf{G}\in\Xi_{\mathrm{E}}^{\mathrm{AP}},\Delta\mathbf{E}\in\Xi_{\mathrm{E}}^{\mathrm{PS}}}\frac{\mathbf{G}^H\mathbf{W}_k\mathbf{G}}{\Gamma_{\mathrm{tol}}}\preceq\mathbf{G}^H(\mathbf{U}+\mathbf{B}_{\mathrm{AP}})\mathbf{G}+\mathbf{E}^H(\mathbf{Z}^H+\mathbf{B}_{\mathrm{PS-II}})\mathbf{E},\quad\forall k,\\
&\widetilde{\mathrm{C4}}\text{: } \tau_{\mathrm{II}}\widetilde{P}_{\mathrm{AP-II}}\leq\tau_{\mathrm{I}}\Xi_{\mathrm{tot}}(\varrho)+E_{\mathrm{res}},\quad\widetilde{\mathrm{C5}}\text{: } \varrho\leq\mathrm{Tr}(\mathbf{L}^H(\mathbf{V}+\mathbf{B}_{\mathrm{PS-I}})\mathbf{L}),\quad\widetilde{\mathrm{C7}},\ \widetilde{\mathrm{C8}},\ \mathrm{C10},\ \mathrm{C11},\\
&\widetilde{\mathrm{C9}}\text{: } \sum_{k=1}^{K}\mathrm{Tr}(\mathbf{W}_k)+\mathrm{Tr}(\mathbf{U})+\sum_{n=1}^{N_{\mathrm{AP}}}\mathrm{Tr}(\mathbf{S}_n\mathbf{B}_{\mathrm{AP}})\leq P_{\max}^{\mathrm{AP}},\\
&\mathrm{C12a}\text{: } \eta_n(a_n)\leq[\mathbf{B}_{\mathrm{AP}}]_{n,n},\quad\forall n,\quad\mathrm{C12b}\text{: } \sum_{k=1}^{K}\mathrm{Tr}(\mathbf{S}_n\mathbf{W}_k)+\mathrm{Tr}(\mathbf{S}_n\mathbf{U})\leq a_n,\quad\forall n,\\
&\mathrm{C13a}\text{: } \eta_m(b_m)\leq[\mathbf{B}_{\mathrm{PS-I}}]_{m,m},\quad\forall m,\quad\mathrm{C13b}\text{: } \mathrm{Tr}(\mathbf{S}_m\mathbf{V})\leq b_m,\quad\forall m,\\
&\mathrm{C14a}\text{: } \eta_m(c_m)\leq[\mathbf{B}_{\mathrm{PS-II}}]_{m,m},\quad\forall m,\quad\mathrm{C14b}\text{: } \mathrm{Tr}(\mathbf{S}_m\mathbf{Z})\leq c_m,\quad\forall m,\\
&\mathrm{C15a}\text{: } \nu(d_k)\leq r_{\mathrm{IR},k},\quad\forall k,\quad\mathrm{C15b}\text{: } \mathrm{Tr}(\mathbf{H}_k(\mathbf{U}+\sum_{i=1}^{K}\mathbf{W}_i)+\mathbf{F}_k\mathbf{Z}))\leq d_k,\quad\forall k,\\
&\mathrm{C16}\text{: } \mathrm{Rank}(\mathbf{W}_k)\leq 1,\quad\forall k,\quad\mathrm{C17}\text{: } \mathbf{W}_k\succeq\mathbf{0},\quad\forall k.
\end{aligned}\tag{25}$$

Next, we handle the infinitely many possibilities in $\widetilde{\mathrm{C2}}$. First, by introducing an auxiliary optimization matrix $\mathbf{N}\in\mathbb{C}^{N_{\mathrm{EV}}\times N_{\mathrm{EV}}}$, constraint $\widetilde{\mathrm{C2}}$ can be equivalently written as:

$$\widetilde{\mathrm{C2a}}\text{: } \max_{\Delta\mathbf{G}\in\Xi_{\mathrm{E}}^{\mathrm{AP}}}\frac{\mathbf{G}^H\mathbf{W}_k\mathbf{G}}{\Gamma_{\mathrm{tol}}}\preceq\mathbf{G}^H(\mathbf{U}+\mathbf{B}_{\mathrm{AP}})\mathbf{G}+\mathbf{N},\quad\forall k,\tag{26}$$

$$\widetilde{\mathrm{C2b}}\text{: } \min_{\Delta\mathbf{E}\in\Xi_{\mathrm{E}}^{\mathrm{PS}}}\ \mathbf{N}\succeq\mathbf{E}^H(\mathbf{Z}+\mathbf{B}_{\mathrm{PS-II}})\mathbf{E}.\tag{27}$$

Then, we introduce a lemma to overcome the infinitely many inequalities in $\widetilde{\mathrm{C2a}}$ and $\widetilde{\mathrm{C2b}}$.

Lemma 1 (Robust Quadratic Matrix Inequalities [41]): Let a quadratic matrix function $f(\mathbf{X})$ be defined as

$$f(\mathbf{X})=\mathbf{X}^H\mathbf{A}\mathbf{X}+\mathbf{X}^H\mathbf{B}+\mathbf{B}^H\mathbf{X}+\mathbf{C},\tag{28}$$

where $\mathbf{X}$, $\mathbf{A}$, $\mathbf{B}$, and $\mathbf{C}$ are arbitrary matrices with appropriate dimensions. Then, the following two statements are equivalent:

$$\begin{aligned}
&f(\mathbf{X})\ \succeq\ \mathbf{0},\quad\forall\mathbf{X}\in\left\{\mathbf{X}\mid\mathrm{Tr}(\mathbf{D}\mathbf{X}\mathbf{X}^H)\leq 1\right\}\\
&\quad\Longleftrightarrow\begin{bmatrix}\mathbf{C}&\mathbf{B}^H\\\mathbf{B}&\mathbf{A}\end{bmatrix}-t\begin{bmatrix}\mathbf{I}&\mathbf{0}\\\mathbf{0}&-\mathbf{D}\end{bmatrix}\succeq\mathbf{0},\quad\text{if }\exists t\geq 0,
\end{aligned}\tag{29}$$

for matrix $\mathbf{D}\succeq\mathbf{0}$ and t is an auxiliary constant.

Then, constraint $\widetilde{\mathrm{C2a}}$ can be equivalently transformed into:

$$\begin{aligned}
&\widetilde{\mathrm{C2a}}\text{: } \mathbf{S}_{\mathrm{C2a}_k}\left(\mathbf{B}_{\mathrm{AP}},\mathbf{U},\mathbf{W}_k,\mathbf{N},t_k\right)\\
&=\begin{bmatrix}\mathbf{N}-t_k\mathbf{I}_{N_{\mathrm{EV}}}&\mathbf{0}\\\mathbf{0}&\frac{t_k\mathbf{I}_{\mathrm{AP}}}{v_{\mathrm{AP}\to\mathrm{E}}^2}\end{bmatrix}+\mathbf{R}_{\widehat{\mathbf{G}}}^H\mathbf{M}_k\mathbf{R}_{\widehat{\mathbf{G}}}\succeq\mathbf{0},\quad\forall k,
\end{aligned}\tag{30}$$

where

$$\mathbf{M}_k=\mathbf{U}+\mathbf{B}_{\mathrm{AP}}-\frac{\mathbf{W}_k}{\Gamma_{\mathrm{tol}}}\quad\text{and }\mathbf{R}_{\widehat{\mathbf{G}}}=[\widehat{\mathbf{G}}\ \mathbf{I}_{\mathrm{AP}}].$$

Similarly, we can transform constraint $\widetilde{\mathrm{C2b}}$ into its equivalent form:

$$\begin{aligned}
&\widetilde{\mathrm{C2b}}:\mathbf{S}_{\mathrm{C2b}}\left(\mathbf{B}_{\mathrm{PS-II}},\mathbf{Z},\mathbf{N},\gamma\right)\\
&=\begin{bmatrix}-\mathbf{N}-\gamma\mathbf{I}_{\mathrm{PS}}&\mathbf{0}\\\mathbf{0}&\frac{\gamma\mathbf{I}_{\mathrm{PS}}}{v_{\mathrm{PS}\to\mathrm{E}}^2}\end{bmatrix}+\mathbf{R}_{\widehat{\mathbf{E}}}^H\mathbf{K}\mathbf{R}_{\widehat{\mathbf{E}}}\succeq\mathbf{0},\quad\forall k,
\end{aligned}\tag{31}$$

where

$$\mathbf{K}=\mathbf{Z}+\mathbf{B}_{\mathrm{PS-II}}\quad\text{and }\mathbf{R}_{\widehat{\mathbf{E}}}=[\widehat{\mathbf{E}}\ \mathbf{I}_{\mathrm{PS}}].$$

Next, we relax the non-convex constraint in C16 by removing it from the problem formulation. Therefore, for a given τ_{I} and τ_{II}, the equivalent SDP relaxed formulation of (21) is given by:

$$\begin{aligned}
&\underset{\varrho,\mathbf{W}_k\in\mathbb{H}^{N_{\mathrm{AP}}},\mathbf{\Lambda},\mathbf{N}\in\mathbb{H}^{N_{\mathrm{EV}}},t_k,\gamma}{\text{minimize}} \quad \tau_{\mathrm{I}}\widetilde{P}_{\mathrm{PS-I}}+\tau_{\mathrm{II}}(\widetilde{P}_{\mathrm{AP-II}}+\widetilde{P}_{\mathrm{PS-II}})\\
&\quad\text{s.t. } \widetilde{\mathrm{C1}},\ \widetilde{\mathrm{C2a}},\ \widetilde{\mathrm{C2b}},\widetilde{\mathrm{C4}},\ \widetilde{\mathrm{C5}},\ \widetilde{\mathrm{C7}}-\widetilde{\mathrm{C9}},\\
&\qquad\mathrm{C10},\mathrm{C11},\mathrm{C12a},\mathrm{C12b},\mathrm{C13a},\mathrm{C13b},\mathrm{C14a},\mathrm{C14b},\\
&\qquad\mathrm{C15a},\mathrm{C15b},\mathrm{C17},\mathrm{C18}:t_k,\gamma\ \geq 0,
\end{aligned}\tag{32}$$

where constraint C18 is due to the use of Lemma 1 for handling the infinitely many constraints associated with the channel estimation errors.

The optimization problem in (32) is a standard convex optimization problem and can be solved efficiently by numerical convex program solvers such as CVX [42]. However, by solving (32) numerically, in general, there is no guarantee that the optimal solution of (32) satisfies C16 of the original problem formulation in (20), i.e., $\mathrm{Rank}(\mathbf{W}_k)\leq 1$. Hence, in the following, we study the structure of the solution of the SDP relaxed problem in (25).

TABLE I
ITERATIVE RESOURCE ALLOCATION ALGORITHM

Algorithm Alternating Optimization

1: Initialize the maximum number of iterations $L_{\max}$ and convergence error tolerance $\psi \to 0$
2: Set iteration index $l = 0$ and initialize $\{\mathcal{P}, \mathbf{W}_k, \mathbf{\Lambda}, \mathbf{N}, t_k, \gamma\}$
3: **repeat** {Loop}
4: Solve (33) for τ_{I} and τ_{II} for given $\{\mathcal{P}', \mathbf{W}'_k, \mathbf{\Lambda}', \mathbf{N}', t'_k, \gamma'\} = \{\mathcal{P}, \mathbf{W}_k, \mathbf{\Lambda}, \mathbf{N}, t_k, \gamma\}$ which leads to intermediate time allocation variables τ'_{I} and τ'_{II}
5: Solve (25) for $\{\mathcal{P}, \mathbf{W}_k, \mathbf{\Lambda}, \mathbf{N}, t_k, \gamma\}$ for given τ'_{I} and τ'_{II} via SDP relaxation and obtain the intermediate solution $\{\mathcal{P}', \mathbf{W}'_k, \mathbf{\Lambda}', \mathbf{N}', t'_k, \gamma'\}$
6: **if** $|\tau'_{\mathrm{I}} - \tau_{\mathrm{I}}(l-1)| \leq \psi$ and $|\tau'_{\mathrm{II}} - \tau_{\mathrm{II}}(l-1)| \leq \psi$ **then**
7: Convergence = **true**
8: **return** $\{\mathcal{P}', \mathbf{W}'_k, \mathbf{\Lambda}', \mathbf{N}', t'_k, \gamma', \tau'_{\mathrm{I}}, \tau'_{\mathrm{II}}\}$
9: **else**
10: $\tau_{\mathrm{I}}(l) = \tau'_{\mathrm{I}}$, $\tau_{\mathrm{II}}(l) = \tau'_{\mathrm{II}}$, $l = l + 1$
11: **end if**
12: **until** $l = L_{\max}$

Theorem 1: Suppose that the optimization problem in (32) is feasible. Then, for $\Gamma_{\mathrm{req}_k} > 0$ and $\Gamma_{\mathrm{tol}} > 0$, the rank-one constraint relaxation of $\mathbf{W}_k$, of the SDP relaxed optimization problem in (32) is tight, i.e., $\mathrm{Rank}(\mathbf{W}_k) = 1, \forall k$. Besides, $\mathrm{Rank}(\mathbf{U}) \leq 1$, $\mathrm{Rank}(\mathbf{Z}) \leq 1$, $\mathrm{Rank}(\mathbf{V}) \leq 1$.

Proof: Please refer to the Appendix.

Theorem 1 states that the globally optimal solution of (32) can be obtained by information beamforming for each IR, despite the HWIs at the transceivers. Moreover, beamforming is also optimal for wireless charging and jamming in Phase I and Phase II, respectively, even when the non-linearity of the EH circuits, the residual HWIs, and the imperfect CSI are taken into account. In summary, we first discretize the continuous optimization variables $\tau_{\mathrm{I}}, \tau_{\mathrm{II}}$. Then, we solve (32) for each pair of $\tau_{\mathrm{I}}, \tau_{\mathrm{II}}$ satisfying $\tau_{\mathrm{I}} + \tau_{\mathrm{II}} \in [0, T_{\max}]$. Finally, we obtain the globally optimal solution[10] of (20) by employing a two-dimensional search over all combinations of $\tau_{\mathrm{I}}, \tau_{\mathrm{II}}$ to find the minimum objective value.

B. Suboptimal Solution

Although the method proposed in the last section achieves the globally optimal solution of (20), it requires a two-dimensional search with respect to optimization variables $\tau_{\mathrm{I}}, \tau_{\mathrm{II}}$ and the number of SDPs to be solved increase quadratically with the resolution of the search grid. To reduce the computational complexity, we propose in the following a suboptimal resource allocation algorithm. In fact, (20) is jointly convex with respect to τ_{I} and τ_{II} when the other optimization variables are fixed. As a result, an iterative alternating optimization method [43] is proposed to obtain a locally optimal solution of (20) and the algorithm is summarized in Table I. The algorithm is implemented by a repeated loop. In line 2, we first set the iteration index l to zero and initialize the resource allocation policy.[11] Variables $\tau_{\mathrm{I}}(l)$ and $\tau_{\mathrm{II}}(l)$ denote the time allocation policy in the l-th iteration. Then, in each iteration, for a given intermediate beamforming policy $\{\mathcal{P}', \mathbf{W}'_k, \mathbf{\Lambda}', \mathbf{N}', t'_k, \gamma'\}$, we solve

$$\begin{aligned} &\underset{\{\tau_{\mathrm{I}}, \tau_{\mathrm{II}}\}}{\text{minimize}} \ \tau_{\mathrm{I}} \widetilde{P}_{\mathrm{PS-I}} + \tau_{\mathrm{II}} (\widetilde{P}_{\mathrm{AP-II}} + \widetilde{P}_{\mathrm{PS-II}}) \\ &\text{s.t. } \widetilde{\mathrm{C1}}, \widetilde{\mathrm{C2a}}, \widetilde{\mathrm{C2b}}, \mathrm{C3}, \widetilde{\mathrm{C4}}, \mathrm{C6}, \end{aligned} \tag{33}$$

c.f., line 4 of Table I. Since (33) is a linear programming (LP) problem, we can solve (33) via the simplex method or any standard numerical solver for solving LPs [44]. The time allocation obtained from (33), i.e., τ'_{I} and τ'_{II}, is used as an input to (25) for solving for $\{\mathcal{P}', \mathbf{W}'_k, \mathbf{\Lambda}', \mathbf{N}', t'_k, \gamma'\}$ via SDP relaxation. Then, we repeat the procedure iteratively until the maximum number of iterations is reached or convergence is achieved. Convergence to a locally optimal solution of (20) is guaranteed for a sufficiently large number of iterations [43], since the considered problem in (25) is convex with respect to the optimization variable sets $\{\tau_{\mathrm{I}}, \tau_{\mathrm{II}}\}$ and $\{\mathcal{P}', \mathbf{W}'_k, \mathbf{\Lambda}', \mathbf{N}', t'_k, \gamma'\}$ individually.

Remark 3: The computational complexity per iteration using a numerical convex program solver for solving an SDP is given by [45]

$$\mathcal{O}\Big(mn^3 + m^2n^2 + m^3\Big), \tag{34}$$

where $\mathcal{O}(\cdot)$ is the big-O notation, m denotes the number of semidefinite cone constraints and n denotes the dimension of the semidefinite cone. In particular, for the problem at hand, m is equivalent to the number of constraints with respect to the semidefinite optimization matrices and n is the total number of antennas in the system. For simplicity, we analyze the computational complexity of the proposed optimal and suboptimal algorithms by assuming $N_{\mathrm{AP}} = N_{\mathrm{PS}} = N$. Hence, the computational complexity of the proposed optimal and suboptimal algorithms with respect to the number of information receivers K is given by[12] [45]

$$\mathcal{O}\left(N_{\mathrm{Grid}}^2 \left(\sqrt{N}\log\left(\frac{1}{\Delta}\right)\right) \times \Big((6N+3K)N^3 + N^2(6N+3K)^2 + (6N+3K)^3\Big)\right) \tag{35}$$

and

$$\mathcal{O}\left(N_{\mathrm{Iter}} \left(\sqrt{N}\log\left(\frac{1}{\Delta}\right)\right) \times \Big((6N+3K)N^3 + N^2(6N+3K)^2 + (6N+3K)^3\Big)\right), \tag{36}$$

respectively, for a given solution accuracy $\Delta > 0$ of the adopted numerical solver, where N_{Grid}^2 is the number of grids required for the two-dimensional search for the optimal values of τ_{I} and τ_{II}, and N_{Iter} is the maximum number of iterations set for the suboptimal algorithm. Note that in general, $N_{\mathrm{Grid}}^2 \gg N_{\mathrm{Iter}}$ holds in practice, and the proposed suboptimal algorithm provides a low-complexity solution for the considered problem [45].

[10] Note that the optimality of this method depends on the resolution of the discretization.

[11] We randomly select a pair of $\{\tau_{\mathrm{I}}, \tau_{\mathrm{II}}\}$ satisfying constraint C3 and solve (25) for $\{\mathcal{P}, \mathbf{W}_k, \mathbf{\Lambda}, \mathbf{N}, t_k, \gamma\}$. The obtained solution is adopted as the initial point for the proposed alternating optimization algorithm.

[12] We note that the computational complexity of the proposed suboptimal algorithm is dominated by the complexity required for solving (25).

TABLE II
SIMULATION PARAMETERS

Carrier center frequency	915 MHz
Bandwidth	200 kHz
Path loss exponent: PS→AP, AP→IRs, PS→Eve, AP→Eve	2, 3.6, 3.6, 3.6
PS to AP fading distribution	Rician, Rician factor 3 dB
AP to IRs, Eve fading distribution	Rayleigh
PS and AP antenna gain	10 dBi and 8 dBi
Noise power	$\sigma_n^2 = \sigma_{\text{IR}}^2 = \sigma_{\text{E}}^2 = -77$ dBm
Power amplifier efficiency	$1/\rho_{\text{PS}} = 1/\rho_{\text{AP}} = 30\,\%$
Circuit power consumption	$P_{\text{C}_{\text{PS}}} = P_{\text{C}_{\text{AP}}} = 50\,\mu$W
Non-linear EH model parameters	$M = 24$ mW, $a = 150$, $b = 0.0014$ [30]
Distance PS-to-AP, PS-to-Eve, AP-to-Eve	10 m, 40 m, 30 m
Maximum transmit power at PS and AP	$P_{\max}^{\text{PS}} = P_{\max}^{\text{AP}} = 30$ dBm

V. SIMULATION

In this section, we evaluate the performance of the proposed optimal and suboptimal resource allocation schemes for the considered WPCN architecture. The relevant simulation parameters are provided in Table II. For conducting the two-dimensional search for the optimal resource allocation, we quantize the possible ranges of τ_{I}, τ_{II}, $0.0001 \leq \tau_{\text{I}}, \tau_{\text{II}} \leq T_{\max}$, into 20×20 equally spaced intervals, and for simplicity, we normalize the duration of the communication slot to $T_{\max} = 1$. Unless specified otherwise, we assume for the transmitter HWI parameters $k_1 = 2.258 \times 10^5$ and $k_2 = 7.687$, and for the receiver distortion parameter $k_3 = 0$. The IRs are randomly distributed at a distance of 50 meters around the AP and the data rate requirements of all IRs are equal, i.e., $R_{\text{req}_k} = R_{\text{req}}$ bit/s, $\forall k$, while the maximum tolerable rate of Eve is $R_{\text{tol}} = 0.1$ bit/s. Besides, we assume $N_{\text{PS}} = 6$, $N_{\text{AP}} = 6$, and $N_{\text{EV}} = 2$ antennas at the PS, AP, and Eve, respectively, unless specified otherwise. For calculating the system power consumption, to avoid counting the same power twice, we consider only the power consumption of Phase I and the power consumed from E_{res} (if any) in Phase II. In the sequel, we define the normalized maximum channel estimation error of the eavesdropper as $\sigma_{\text{EVE}}^2 = 1\% \geq \frac{v_{\text{AP}\to\text{E}}^2}{\|\mathbf{G}\|_{\text{F}}^2}, \frac{v_{\text{PS}\to\text{E}}^2}{\|\mathbf{E}\|_{\text{F}}^2}$. Besides, the results shown in this section were averaged over 10,000 fading channel realizations.

A. Convergence of Iterative Suboptimal Algorithm

Figure 3 illustrates the convergence behavior of the proposed iterative suboptimal algorithm for different numbers of antennas equipped at the PS and the AP. We set the minimum required data rate per IR to $R_{\text{req}} = 8$ bits/s/Hz. As can be observed, the proposed iterative suboptimal algorithm converges within 10 iterations on average for all considered scenarios. In particular, the performance of the suboptimal scheme closely approaches that of the optimal scheme. On the other hand, the numbers of antennas equipped at the AP and the PS have only a small impact on the speed of convergence.

In the sequel, for studying the system performance, we set the number of iterations for the proposed suboptimal algorithm to 10.

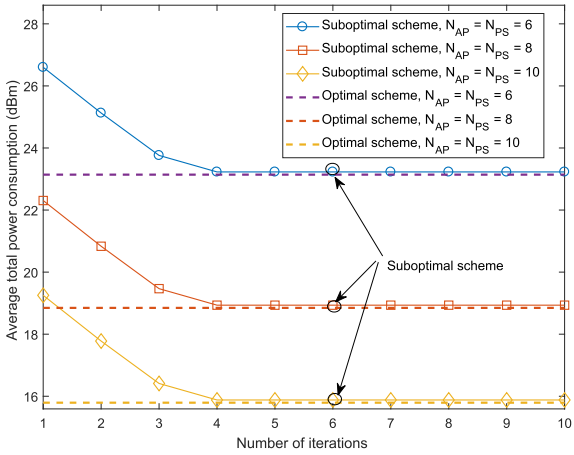

Fig. 3. Average total power consumption (dBm) versus the number of iterations for different numbers of antennas equipped at the PS and the AP.

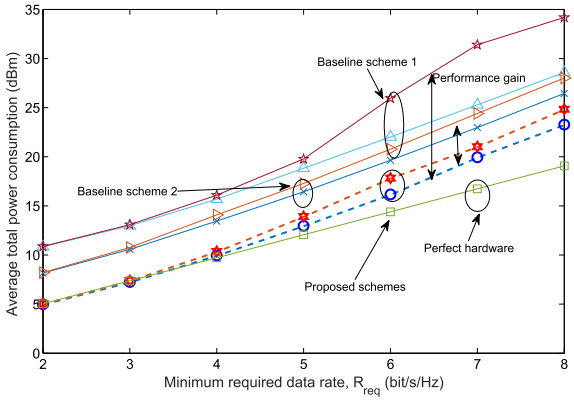

Fig. 4. Average total power consumption (dBm) versus minimum required data rate per IR, R_{req}, for different values of receiver HWI parameter, k_3. The double-sided arrows indicate the power saving due to the proposed optimization.

B. Average Total Transmit Power Versus Minimum Required Rate

In Figure 4, we show the total average power consumption versus the minimum required data rate per IR, R_{req}, for different values of receiver HWI parameter, k_3. Zero residual energy is assumed, i.e., $E_{\text{res}} = 0$. As can be seen from Figure 4,

the total average power consumption of the proposed optimal and suboptimal schemes increases monotonically with R_{req}. The reasons behind this are twofold. First, a higher transmit power for the information signals, $\mathbf{w}_k s_k$, ' is necessary in order to meet more stringent requirements on the minimum data rate. Second, more power has to be allocated to the artificial noise, $\mathbf{z}$, for neutralizing the increased information leakage due to the higher power of $\mathbf{w}_k s_k$. Hence, the PS has to increase the transmit power for wireless charging in Phase I to ensure that a sufficient amount of energy is available for wireless information transfer and artificial noise generation in Phase II. Besides, it can be observed that the average total power consumption increases for increasing receiver HWI parameter, k_3. In fact, for the same amount of received power, the received SINR deteriorates if the receiver HWI parameter, k_3, is increased. Hence, the AP has to sacrifice some spatial degrees of freedom used for mitigation of the multiuser interference received at each IR to alleviate the impact of the receiver HWIs. As a result, it becomes more challenging for the AP to focus the energy of the information signals on the IRs which results in a higher transmit power in Phase I and Phase II. On the other hand, although only 10 iterations are used, the proposed suboptimal scheme performs close to the optimal scheme employing the two-dimensional exhaustive search.

For comparison, Figure 4 also contains the performance of one benchmark scheme and three baseline schemes. For the benchmark scheme, we assume that perfect hardware is available at all transceivers of the considered WPCN, i.e., there are no HWIs, and the corresponding performance serves as an upper bound for the proposed schemes. For baseline 1, we set $P_{\max}^{\text{PS}} = P_{\max}^{\text{AP}} = 40$ dBm. Then, we solve (20) with the proposed optimal resource allocation algorithm but adopt a fixed isotropic radiation pattern for $\mathbf{V}$. For baseline 2, resource allocation is performed subject to the same constraint set as in (20), except that the linear energy harvesting model [5] assuming a constant energy conversion efficiency $\eta = 0.5$ is considered. The performance of baseline 2 is then evaluated for the considered WPCN with non-linear energy harvesting circuits. We also considered a baseline 3 where resource allocation was performed subject to the same constraint set as in (20), except that the residual HWIs at the transceivers were not taken into account. The performance of baseline 3 was then evaluated in the presence of the residual HWIs. However, for the adopted simulation settings, baseline 3 could not satisfy the QoS requirements specified by constraints C1 and C2 as the residual HWIs were ignored in the design phase. Therefore, performance results for baseline 3 are not shown in Figure 4. This underlines the importance of taking residual HWIs into account for resource allocation design. On the other hand, as expected, the performance gap between the scheme with the perfect hardware and the proposed schemes is slightly enlarged as R_{req} increases. In fact, the interference caused by the transmitter and receiver HWIs increases with the transmit power and the received power, respectively. Hence, a higher data rate requirement, R_{req}, magnifies the impact of the HWIs on system performance. Furthermore, as can be observed from Figure 4, baseline 1 consumes a significantly higher power compared to the proposed schemes. This is because baseline 1 is less efficient in wireless charging compared to the proposed schemes. In particular, the PS and the AP cannot fully utilize the available degrees of freedom since the direction of the transmit energy signal at the PS in Phase I is fixed. The resulting performance gap reveals the importance of optimizing all beamforming matrices for the minimization of the total power consumption of the considered WPCN. Besides, it can be observed that the proposed optimal and suboptimal algorithms provide substantial power consumption savings compared to baseline 2, particularly when the HWIs are severe. In fact, baseline 2 causes a mismatch in resource allocation since it does not account for the non-linearity of the energy harvesting circuits.

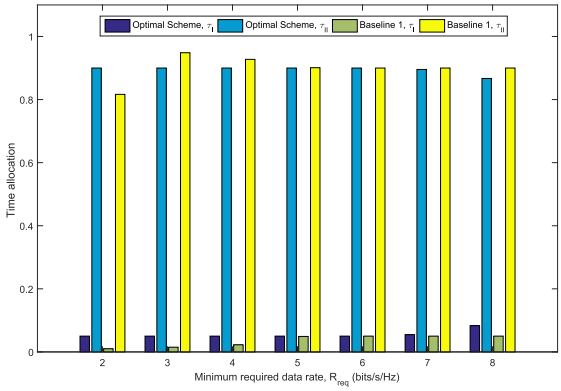

Fig. 5. Average power allocation (dBm) versus minimum required data rate per IR, R_{req}, for $k_3 = 0$.

In Figures 5 and 6, we depict the time allocation and power allocation of the proposed schemes and baseline 1 for the scenario with $k_3 = 0$ studied in Figure 4. In particular, Figure 6 shows the average transmit powers allocated to the three components[13] of the transmitted signals, i.e., $\sum_{k=1}^{K} \text{Tr}(\mathbf{W}_k)$, $\text{Tr}(\mathbf{V})$, and $\text{Tr}(\mathbf{Z})$. First, it can be observed from Figure 5 that the time allocated[14] to Phase I for wireless charging in the considered WPCN is monotonically increasing with respect to the minimum data rate requirement per IR. In fact, the system increases both the transmit power and the time duration allocated to the PS in Phase I to enable a more effective wireless charging of the AP as the data rate requirement becomes more stringent. Besides, for all considered values of R_{req}, it can be seen that a small portion of time is allocated for wireless charging while a large portion of time is reserved for wireless information transfer. Recall that the equivalent minimum required SINR at IR k is defined as $\Gamma_{\text{req}_k} = 2^{R_{\text{req}_k}/\tau_{\text{II}}} - 1$. Hence, increasing the value of τ_{II} can effectively lower the required equivalent SINR so as to reduce the total system power consumption. On the other hand, as expected, the amounts of power allocated to the information signals and the energy/artificial noise signals, $\mathbf{v}, \mathbf{z}$, increase for the proposed schemes as the minimum required data rate per IR R_{req} increases. In particular, the power allocated to

[13] Since $\text{Tr}(\mathbf{U}) = 0$ in all the considered cases, it is not shown in Figure 6.

[14] Note that the time allocation for the proposed suboptimal scheme is similar to that of the optimal scheme, and hence, is omitted for brevity.

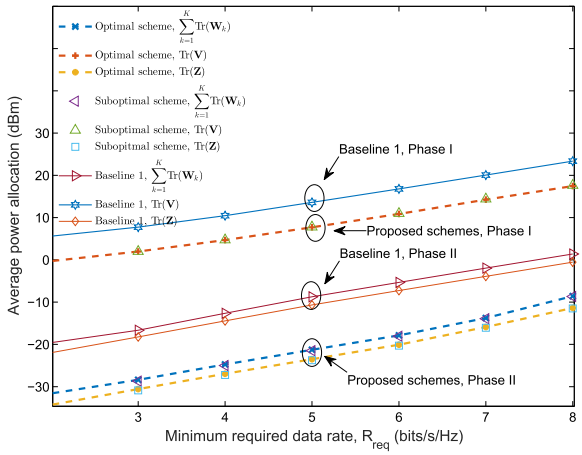

Fig. 6. Average power allocation (dBm) versus minimum required data rate per IR, R_{req}, for $k_3 = 0$.

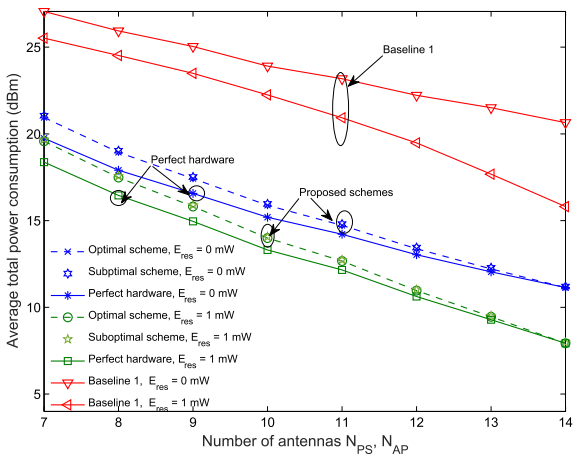

Fig. 7. Average total power consumption (dBm) versus the numbers of antennas equipped at the PS and the AP, N_{AP} and N_{PS}, for different amounts of available residual energy E_{res}.

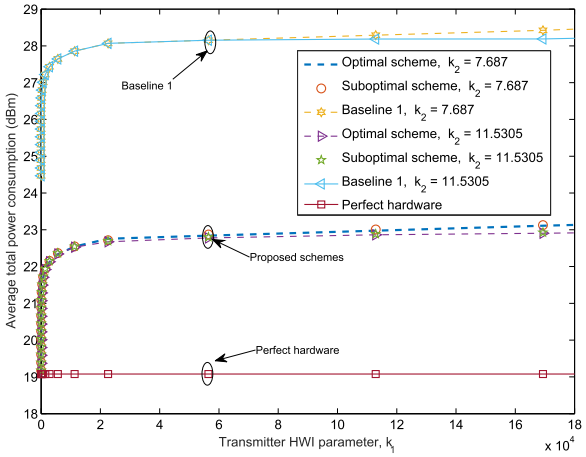

Fig. 8. Average total power consumption (dBm) versus the transmitter HWI parameter, k_1, for different values of k_2.

the energy/artificial noise signals, $\mathbf{v}, \mathbf{z}$, increases as fast as the power allocated to the information signals when R_{req} increases. This is because for a more stringent data rate requirement, a higher transmit power is needed for information transmission, and thus, the considered WPCN system is more vulnerable to eavesdropping. Hence, also more energy has to be allocated to the energy/artificial noise signals for more effective wireless charging and jamming. Interestingly, $\mathrm{Tr}(\mathbf{U}) = 0$ holds for all considered values of the required data rate which suggests that generating artificial noise at the AP for jamming is not beneficial. In fact, transmitting artificial noise from the AP for ensuring communication security is less power efficient than transmitting the artificial noise directly from the PS. The reasons for this are twofold. First, the non-linearity of the energy harvesting circuits limits the maximum amount of harvestable energy for generating a strong jamming signal at the AP. Second, since $E_{\mathrm{res}} = 0$, all energy consumed at the AP has to be harvested first from the RF signals transmitted by the PS. As a result, if the AP utilizes the energy harvested in Phase I to generate a jamming signal in Phase II, the energy of the jamming signal is subject to the attenuation of both the PS-to-AP link and the AP-to-Eve link before reaching the potential eavesdropper. Such a "double energy attenuation" severely decreases the efficiency of communication security provisioning, and thus is avoided by the optimal resource allocation scheme.

In Figure 7, we show the average total power consumption versus the number of antennas equipped at the PS and the AP for different resource allocation schemes. The minimum required data rate of the IRs is set to $R_{\mathrm{req}} = 8$ bits/s/Hz. For simplicity, we assume that $N_{\mathrm{AP}} = N_{\mathrm{PS}}$. As can be seen from Figure 7, the total transmit power decreases with increasing numbers of antennas. In fact, the extra degrees of freedom offered by increasing numbers of antennas can be exploited for more efficient resource allocation. Specifically, with more antennas, the direction of beamforming matrices $\mathbf{V}$ and $\mathbf{W}_k$ can be more accurately steered towards the AP and IR k, respectively, which substantially reduces the transmit power required in Phase I and Phase II, respectively, for satisfying the data rate requirement. Besides, the additional antennas at the AP serve as additional wireless energy collectors for energy harvesting which substantially improves the efficiency of energy harvesting at the AP. Also, the proposed schemes provide substantial power savings compared to baseline 1 due to the proposed optimization. Furthermore, the performance gap between the case of perfect hardware and the proposed schemes diminishes as the numbers of antennas equipped at the AP and PS increase, since a lower transmit power and more accurate beamforming alleviate the impact of transmit and receive HWIs, respectively. On the other hand, a higher amount of residual energy E_{res} reduces the total power consumption of the system. Indeed, less PS transmit power is required for wireless charging in Phase I when the AP is equipped with a certain amount of residual energy E_{res}. This also substantially reduces the power waste due to the high signal propagation loss in wireless charging in Phase I.

Figure 8 depicts the average total power consumption versus the transmitter HWI parameter k_1 for the proposed optimal and suboptimal resource allocation schemes for different values of k_2. The residual energy and the minimum required data rate are set to $E_{\mathrm{res}} = 0$ and $R_{\mathrm{min}} = 8$ bit/s/Hz, respectively.

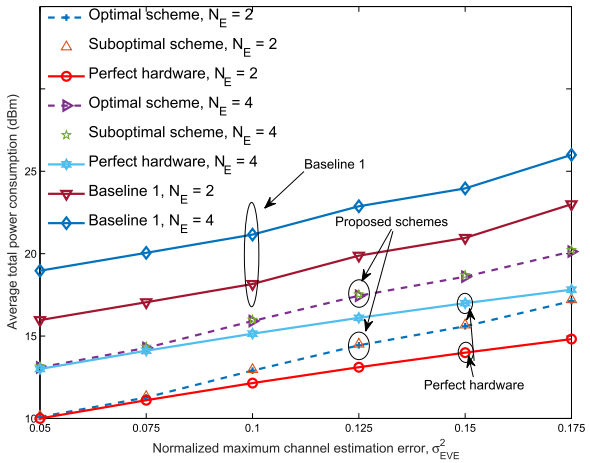

Fig. 9. Average total power consumption (dBm) versus the normalized maximum channel estimation error for different numbers of antennas equipped at the eavesdropper, N_{E}.

As can be observed, the power consumption of the system increases with the transmitter HWI parameter k_1. This is because the power waste in (17)-(19) increases when the transmitter HWIs become more severe leading to a less efficient resource allocation. Besides, the system power consumption of the proposed optimal and suboptimal schemes decreases with increasing k_2. As a matter of fact, when the transmit power is properly controlled below 1 watt, cf. (6), increasing k_2 decreases the power waste caused by HWIs. On the other hand, the system power consumption of the proposed schemes is significantly lower than that of baseline 1. Besides, for the scheme with perfect hardware, the performance is independent of the HWI levels, of course, and serves as an upper bound for the proposed schemes.

In Figure 9, we show the average total power consumption of the system versus the normalized maximum channel estimation error. The minimum required data rate of the IRs is set to $R_{\mathrm{req}} = 4$ bits/s/Hz. As can be observed, the average total power consumption increases with increasing maximum channel estimation error for all considered schemes. In fact, as the imperfectness of the CSI increases, both the AP and the PS become less capable of exploiting the available spatial degrees of freedom efficiently for resource allocation. As a result, the PS has to allocate more power to the artificial noise, $\mathbf{z}$, to prevent interception by the eavesdropper so as to fulfill constraint C2. Besides, the proposed schemes provide a substantial system power saving compared to baseline 1, despite the imperfect CSI. Furthermore, the performance gap between the proposed schemes and the scheme with perfect hardware increases as the CSI knowledge becomes less accurate. In fact, the higher transmit power needed in the presence of imperfect CSI at both the PS and AP to fulfill the QoS requirement worsens the impact of the HWIs. On the other hand, more power is consumed if the eavesdropper is equipped with more antennas. This is attributed to the fact that the eavesdropping capability of the eavesdropper improves with N_{E}. To still guarantee communication security, the PS has to allocate more power to the artificial noise which leads to a higher system power consumption.

VI. Conclusions

In this paper, we studied the power-efficient resource allocation algorithm design for providing communication secrecy in WPCNs, where we took into account a practical non-linear EH model and the residual HWIs at the transceivers. The resource allocation algorithm design was formulated as a non-convex optimization problem for the minimization of the total consumed power subject to QoS constraints at the IRs. The optimal solution of the design problem was obtained via a two-dimensional search and SDP relaxation. Besides, a low computational complexity suboptimal solution was also provided. Numerical results demonstrated the detrimental effects of residual HWIs on performance in WPCNs. Furthermore, although residual HWIs limit the system performance in the high transmit/receive power regimes, the resulting performance degradation can be effectively alleviated by increasing the number of antennas in the system and by acquiring more accurate CSI of the eavesdropper.

Appendix
Proof of Theorem 1

The proof is divided into two parts. In the first part, we study the rank of the information beamforming matrix, $\mathbf{W}_k, \forall k$. Then, we investigate the ranks of energy beamforming matrices $\mathbf{V}$, $\mathbf{U}$, and $\mathbf{Z}$ in the second part. Since the SDP relaxed problem in (32) satisfies Slater's constraint qualification and is jointly convex with respect to the optimization variables, strong duality holds and we can exploit the dual problem [44] in order to study the structure of the solution of the primal problem. To this end, we write the Lagrangian function of (32) as:

$$\begin{aligned}\mathcal{L} = {} & (\rho_{\mathrm{AP}}\tau_{\mathrm{II}} + \vartheta)\Big(\sum_{k=1}^{K}\mathrm{Tr}\left(\mathbf{W}_k\right)\Big) + (\psi + \rho_{\mathrm{PS}}\tau_{\mathrm{I}})\,\mathrm{Tr}\left(\mathbf{V}\right) \\ & - \beta\Big(\mathrm{Tr}(\mathbf{L}^H\mathbf{V}\mathbf{L})\Big) + \sum_{k=1}^{K}\theta_k\Big(\mathrm{Tr}(\mathbf{H}_k\sum_{i=1}^{K}\mathbf{W}_i)\Big) - \mathrm{Tr}\left(\mathbf{D}_{\mathrm{C}10}\mathbf{V}\right) \\ & + \sum_{k=1}^{K}\lambda_k\Big(\sum_{j\neq k}\mathrm{Tr}\left(\mathbf{H}_k\mathbf{W}_j\right) - \frac{\mathrm{Tr}\left(\mathbf{H}_k\mathbf{W}_k\right)}{\Gamma_{\mathrm{req}}}\Big) \\ & - \sum_{k=1}^{K}\mathrm{Tr}\left(\mathbf{D}_{\mathrm{C}17_k}\mathbf{W}_k\right) + \sum_{n=1}^{N_{\mathrm{AP}}}\varphi_n\Big(\sum_{k=1}^{K}\mathrm{Tr}(\mathbf{S}_n\mathbf{W}_k)\Big) \\ & - \sum_{k=1}^{K}\mathrm{Tr}\left(\mathbf{D}_{\mathrm{C}2\mathrm{a}_k}\mathbf{S}_{\mathrm{C}2\mathrm{a}_k}\left(\mathbf{B}_{\mathrm{AP}},\mathbf{U},\mathbf{W}_k,\mathbf{N},t_k\right)\right) \\ & + \sum_{m=1}^{N_{\mathrm{PS}}}\chi_m\Big(\mathrm{Tr}(\mathbf{S}_m\mathbf{V}) - b_m\Big) + \Delta\,, \end{aligned} \tag{37}$$

where variables λ_k, β, ψ, ϑ, φ_n, χ_m, and θ_k are the non-negative Lagrange multipliers associated with constraints $\widetilde{\mathrm{C1}}$, $\widetilde{\mathrm{C5}}$, $\widetilde{\mathrm{C7}}$, $\widetilde{\mathrm{C9}}$, C12b, C13b, and C15b, respectively. Moreover, $\mathbf{D}_{\mathrm{C}2\mathrm{a}_k} \succeq \mathbf{0}, \forall k$, $\mathbf{D}_{\mathrm{C}_{10}} \succeq \mathbf{0}$, and $\mathbf{D}_{\mathrm{C}17_k} \succeq \mathbf{0}, \forall k$, are the Lagrangian multiplier matrices corresponding to constraints $\widetilde{\mathrm{C2a}}$, C10, and C17, respectively. Δ denotes the collection

of terms not relevant for the proof. The Karush-Kuhn-Tucker (KKT) conditions needed for the proof are given by[15]:

$$\mathbf{D}^*_{\mathrm{C2a}_k} \succeq \mathbf{0}, \quad \forall k, \ \mathbf{D}^*_{\mathrm{C10}} \succeq \mathbf{0}, \ \mathbf{D}^*_{\mathrm{C17}_k} \succeq \mathbf{0}, \ \forall k, \tag{38}$$

$$\beta^*, \lambda^*_k, \vartheta^*, \psi^*, \varphi^*_n, \theta^*_k, \chi^*_m \geq 0, \tag{39}$$

$$\mathbf{D}^*_{\mathrm{C17}_k}\mathbf{W}^*_k = \mathbf{0}, \quad \forall k, \ \mathbf{D}^*_{\mathrm{C10}}\mathbf{V}^* = \mathbf{0}, \tag{40}$$

$$\nabla_{\mathbf{W}^*_k}\mathcal{L} = \mathbf{0}, \quad \forall k, \quad \nabla_{\mathbf{V}^*}\mathcal{L} = \mathbf{0}. \tag{41}$$

Now, we investigate the rank of $\mathbf{W}^*_k$. From the complementary slackness conditions in (40), we know that the columns of $\mathbf{W}^*_k$ lie in the null space of $\mathbf{D}^*_{\mathrm{C17}_k}$. Hence, we focus on studying the range space of $\mathbf{D}^*_{\mathrm{C17}_k}$ for revealing the structure of $\mathbf{W}^*_k$. By exploiting the KKT conditions in (41), after some mathematical manipulations, we obtain:

$$\mathbf{D}^*_{\mathrm{C17}_k} = \mathbf{\Phi}_k - \lambda^*_k \frac{\mathbf{H}_k}{\Gamma_{\mathrm{req}_k}}, \tag{42}$$

where

$$\mathbf{\Phi}_k = \rho_{\mathrm{AP}}\tau_{\mathrm{II}}\mathbf{I}_k + \sum_{j\neq k}\lambda^*_j\mathbf{H}_j + \frac{\mathbf{R}_{\widehat{\mathbf{G}}}\mathbf{D}^*_{\mathrm{C2a}_k}\mathbf{R}^H_{\widehat{\mathbf{G}}}}{\Gamma_{\mathrm{tol}}} + \sum_{n=1}^{N_{\mathrm{AP}}}\varphi_n\mathbf{S}_n + \sum_{k=1}^{K}\theta_k\mathbf{H}_k \succ \mathbf{0}\,.$$

Then, we study the rank of $\mathbf{D}^*_{\mathrm{C17}_k}$ for $\tau_{\mathrm{II}} > 0$ by exploiting (42) which yields:

$$\mathrm{Rank}\left(\mathbf{D}^*_{\mathrm{C17}_k} + \lambda^*_k\frac{\mathbf{H}_k}{\Gamma_{\mathrm{req}_k}}\right) = \mathrm{Rank}(\mathbf{\Phi}_k) = N_{\mathrm{AP}} \tag{43}$$

$$\Rightarrow \mathrm{Rank}\left(\mathbf{D}^*_{\mathrm{C17}_k}\right) + \mathrm{Rank}\left(\lambda^*_k\frac{\mathbf{H}_k}{\Gamma_{\mathrm{req}_k}}\right) \tag{44}$$

$$\overset{(a)}{\geq} \mathrm{Rank}\left(\mathbf{D}^*_{\mathrm{C17}_k} + \lambda^*_k\frac{\mathbf{H}_k}{\Gamma_{\mathrm{req}_k}}\right) = N_{\mathrm{AP}} \tag{45}$$

$$\overset{(b)}{\Rightarrow} \mathrm{Rank}\left(\mathbf{D}^*_{\mathrm{C17}_k}\right) \geq N_{\mathrm{AP}} - 1, \tag{46}$$

where (a) is due to a basic rank inequality and (b) is due to $\lambda^*_k > 0$ at the optimal solution. Since $\mathrm{Rank}\left(\mathbf{D}^*_{\mathrm{C17}_k}\right) \geq N_{\mathrm{AP}} - 1$, in order to satisfy (40), it is required that $\mathrm{Rank}\left(\mathbf{W}^*_k\right) \leq 1$. In other words, either $\mathbf{W}^*_k = \mathbf{0}$ or $\mathrm{Rank}(\mathbf{W}^*_k) = 1$. On the other hand, $\Gamma_{\mathrm{req}_k} > 0, \forall k$, and hence $\mathbf{W}^*_k \neq \mathbf{0}$. As a result, $\mathrm{Rank}(\mathbf{W}^*_k) = 1$ holds at the optimal solution of the SDP relaxed problem in (25). This completes the proof of the first part.

In the second part, we show $\mathrm{Rank}(\mathbf{V}^*) \leq 1$. By exploiting (41), we have the following equation:

$$\mathbf{D}^*_{\mathrm{C10}} = \rho_{\mathrm{PS}}\tau_{\mathrm{II}}\mathbf{I}_{\mathrm{PS}} + \sum_{m=1}^{N_{\mathrm{AP}}}\chi^*_m\mathbf{S}_m - \beta^*\mathbf{L}\mathbf{L}^H. \tag{47}$$

Since matrix $\mathbf{D}^*_{\mathrm{C10}}$ is positive semidefinite, the following inequalities must hold

$$\lambda_{\max}\left(\frac{\rho_{\mathrm{PS}}\tau_{\mathrm{II}}\mathbf{I}_{\mathrm{PS}} + \sum_{m=1}^{N_{\mathrm{AP}}}\chi^*_m\mathbf{S}_m}{\beta^*}\right) \geq \lambda^{\max}_{\mathbf{L}\mathbf{L}^H} \geq 0, \tag{48}$$

where $\lambda^{\max}_{\mathbf{L}\mathbf{L}^H}$ is the real-valued maximum eigenvalue of matrix $\mathbf{L}\mathbf{L}^H$ and $\beta^* > 0$ at the optimal solution. If $\lambda_{\max}\left(\frac{\rho_{\mathrm{PS}}\tau_{\mathrm{II}}\mathbf{I}_{\mathrm{PS}}+\sum_{m=1}^{N_{\mathrm{AP}}}\chi^*_m\mathbf{S}_m}{\beta^*}\right) > \lambda^{\max}_{\mathbf{L}\mathbf{L}^H}$, $\mathbf{D}^*_{\mathrm{C10}}$ will become positive definite and a full rank matrix, i.e., $\mathrm{Rank}(\mathbf{D}^*_{\mathrm{C10}}) = N_{\mathrm{PS}}$. Thus, to satisfy the complementary slackness condition in (40), $\mathbf{V}^* = \mathbf{0}$ or $\mathrm{Rank}(\mathbf{V}^*) \leq 1$ holds at the optimal solution.[16]

On the other hand, if $\lambda_{\max}\left(\frac{\rho_{\mathrm{PS}}\tau_{\mathrm{II}}\mathbf{I}_{\mathrm{PS}}+\sum_{m=1}^{N_{\mathrm{AP}}}\chi^*_m\mathbf{S}_m}{\beta^*}\right) = \lambda^{\max}_{\mathbf{L}\mathbf{L}^H}$, in order to have a bounded optimal dual solution, it follows that the null space of $\mathbf{D}^*_{\mathrm{C10}}$ is spanned by a vector $\mathbf{u}^{\max}_{\mathbf{L}\mathbf{L}^H}$, which is the unit norm eigenvector of $\mathbf{L}\mathbf{L}^H$ associated with eigenvalue $\lambda^{\max}_{\mathbf{L}\mathbf{L}^H}$. Hence, $\mathrm{Rank}(\mathbf{D}^*_{\mathrm{C10}}) \geq N_{\mathrm{PS}} - 1$. By using a similar approach as in the first part of this proof for proving $\mathrm{Rank}(\mathbf{W}^*_k) = 1$, we can show that $\mathrm{Rank}(\mathbf{V}^*) \leq 1$.

As for proving $\mathrm{Rank}(\mathbf{U}^*) \leq 1$ and $\mathrm{Rank}(\mathbf{Z}^*) \leq 1$, we can follow the same approach as in the second part of this proof. The details are omitted here due to page limitation. ■

[15] We denote the optimal solution for optimization variable x by x^*.

[16] In practice, the solution of $\mathbf{V}^* = \mathbf{0}$ corresponds to the case when E_{res} is sufficiently large and hence Phase I for wireless charging is not necessary.

REFERENCES

[1] E. Boshkovska, D. W. K. Ng, and R. Schober, "Power-efficient and secure WPCNs with residual hardware impairments and a non-linear EH model," in *Proc. IEEE Global Telecommun. Conf.*, 2017, pp. 1–7.

[2] S. Bi, Y. Zeng, and R. Zhang, "Wireless powered communication networks: An overview," *IEEE Wireless Commun.*, vol. 23, no. 2, pp. 10–18, Apr. 2016.

[3] M. Zorzi, A. Gluhak, S. Lange, and A. Bassi, "From today's Intranet of Things to a future Internet of Things: A wireless- and mobility-related view," *IEEE Wireless Commun.*, vol. 17, no. 6, pp. 44–51, Dec. 2010.

[4] Q. Wu, M. Tao, D. W. K. Ng, W. Chen, and R. Schober, "Energy-efficient resource allocation for wireless powered communication networks," *IEEE Trans. Wireless Commun.*, vol. 15, no. 3, pp. 2312–2327, Mar. 2016.

[5] H. Ju and R. Zhang, "Throughput maximization in wireless powered communication networks," *IEEE Trans. Wireless Commun.*, vol. 13, no. 1, pp. 418–428, Jan. 2014.

[6] H. Chen, Y. Li, J. L. Rebelatto, B. F. Uchôa-Filho, and B. Vucetic, "Harvest-then-cooperate: Wireless-powered cooperative communications," *IEEE Trans. Signal Process.*, vol. 63, no. 7, pp. 1700–1711, Apr. 2015.

[7] I. Krikidis, S. Timotheou, S. Nikolaou, G. Zheng, D. W. K. Ng, and R. Schober, "Simultaneous wireless information and power transfer in modern communication systems," *IEEE Commun. Mag.*, vol. 52, no. 11, pp. 104–110, Nov. 2014.

[8] X. Chen, Z. Zhang, H.-H. Chen, and H. Zhang, "Enhancing wireless information and power transfer by exploiting multi-antenna techniques," *IEEE Commun. Mag.*, vol. 53, no. 4, pp. 133–141, Apr. 2015.

[9] Z. Ding *et al.*, "Application of smart antenna technologies in simultaneous wireless information and power transfer," *IEEE Commun. Mag.*, vol. 53, no. 4, pp. 86–93, Apr. 2015.

[10] J. Zhang, L. Dai, S. Sun, and Z. Wang, "On the spectral efficiency of massive MIMO systems with low-resolution ADCs," *IEEE Commun. Lett.*, vol. 20, no. 5, pp. 842–845, May 2016.

[11] E. Björnson, P. Zetterberg, and M. Bengtsson, "Optimal coordinated beamforming in the multicell downlink with transceiver impairments," in *Proc. IEEE Global Telecommun. Conf.*, Dec. 2012, pp. 4775–4780.

[12] J. Zhang, L. Dai, X. Zhang, E. Björnson, and Z. Wang, "Achievable rate of Rician large-scale MIMO channels with transceiver hardware impairments," *IEEE Trans. Veh. Technol.*, vol. 65, no. 10, pp. 8800–8806, Oct. 2016.

[13] C. Studer, M. Wenk, and A. Burg, "MIMO transmission with residual transmit-RF impairments," in *Proc. Int. ITG Workshop Smart Antennas (WSA)*, Feb. 2010, pp. 189–196.

[14] J. Zhang, X. Xue, E. Björnson, B. Ai, and S. Jin, "Spectral efficiency of multipair massive MIMO two-way relaying with hardware impairments," *IEEE Wireless Commun. Lett.*, to be published.

[15] E. Björnson and E. Jorswieck, "Optimal resource allocation in coordinated multi-cell systems," *Found. Trends Commun. Inf. Theory*, vol. 9, nos. 2–3, pp. 113–381, 2013.
[16] X. Chen, D. W. K. Ng, and H.-H. Chen, "Secrecy wireless information and power transfer: Challenges and opportunities," *IEEE Wireless Commun.*, vol. 23, no. 2, pp. 54–61, Apr. 2016.
[17] M. Liu and Y. Liu, "Power allocation for secure SWIPT systems with wireless-powered cooperative jamming," *IEEE Commun. Lett.*, vol. 21, no. 6, pp. 1353–1356, Jun. 2017.
[18] Y. Wu, X. Chen, C. Yuen, and C. Zhong, "Robust resource allocation for secrecy wireless powered communication networks," *IEEE Commun. Lett.*, vol. 20, no. 12, pp. 2430–2433, Dec. 2016.
[19] D. W. K. Ng and R. Schober, "Secure and green SWIPT in distributed antenna networks with limited backhaul capacity," *IEEE Trans. Wireless Commun.*, vol. 14, no. 9, pp. 5082–5097, Sep. 2015.
[20] X. Chen, J. Chen, and T. Liu, "Secure transmission in wireless powered massive MIMO relaying systems: Performance analysis and optimization," *IEEE Trans. Veh. Technol.*, vol. 65, no. 10, pp. 8025–8035, Oct. 2016.
[21] W. Liu, X. Zhou, S. Durrani, and P. Popovski, "Secure communication with a wireless-powered friendly jammer," *IEEE Trans. Wireless Commun.*, vol. 15, no. 1, pp. 401–415, Jan. 2016.
[22] H. Niu, D. Guo, Y. Huang, and B. Zhang, "Robust energy efficiency optimization for secure MIMO SWIPT systems with non-linear EH model," *IEEE Commun. Lett.*, vol. 21, no. 12, pp. 2610–2613, Dec. 2017.
[23] H. Niu, D. Guo, Y. Huang, B. Zhang, and B. Gao, "Outage constrained robust energy harvesting maximization for secure MIMO SWIPT systems," *IEEE Wireless Commun. Lett.*, vol. 6, no. 5, pp. 614–617, Oct. 2017.
[24] H. Niu, B. Zhang, D. Guo, and Y. Huang, "Joint robust design for secure AF relay networks with SWIPT," *IEEE Access*, vol. 5, pp. 9369–9377, Apr. 2017.
[25] Y. Bi and H. Chen, "Accumulate and jam: Towards secure communication via a wireless-powered full-duplex jammer," *IEEE J. Sel. Topics Signal Process.*, vol. 10, no. 8, pp. 1538–1550, Dec. 2016.
[26] J. Moon, H. Lee, C. Song, and I. Lee, "Secrecy performance optimization for wireless powered communication networks with an energy harvesting jammer," *IEEE Trans. Commun.*, vol. 65, no. 2, pp. 764–774, Feb. 2017.
[27] J. Zhu, D. W. K. Ng, N. Wang, R. Schober, and V. K. Bhargava, "Analysis and design of secure massive MIMO systems in the presence of hardware impairments," *IEEE Trans. Wireless Commun.*, vol. 16, no. 3, pp. 2001–2016, Mar. 2017.
[28] D. K. Nguyen, M. Matthaiou, T. Q. Duong, and H. Ochi, "RF energy harvesting two-way cognitive DF relaying with transceiver impairments," in *Proc. IEEE Int. Conf. Commun. Workshop (ICCW)*, Jun. 2015, pp. 1970–1975.
[29] J. Zhu, Y. Li, N. Wang, and W. Xu, "Wireless information and power transfer in secure massive MIMO downlink with phase noise," *IEEE Wireless Commun. Lett.*, vol. 6, no. 3, pp. 298–301, Jun. 2017.
[30] J. Guo and X. Zhu, "An improved analytical model for RF-DC conversion efficiency in microwave rectifiers," in *IEEE MTT-S Int. Microw. Symp. Dig.*, Jun. 2012, pp. 1–3.
[31] T. Schenk, *RF Imperfections in High-Rate Wireless Systems: Impact and Digital Compensation*. New York, NY, USA: Springer, 2010.
[32] "LTE performance vs. output power, model: HXG-122+," Minicircuits.com, New York, NY, USA, Tech. Note AN-60-050. [Online]. Available: http://www.minicircuits.com/app/AN60-050.pdf
[33] E. Boshkovska, D. W. K. Ng, N. Zlatanov, and R. Schober, "Practical non-linear energy harvesting model and resource allocation for SWIPT systems," *IEEE Commun. Lett.*, vol. 19, no. 12, pp. 2082–2085, Dec. 2015.
[34] E. Boshkovska, D. W. K. Ng, N. Zlatanov, A. Koelpin, and R. Schober, "Robust resource allocation for MIMO wireless powered communication networks based on a non-linear EH model," *IEEE Trans. Commun.*, vol. 65, no. 5, pp. 1984–1999, May 2017.
[35] E. Boshkovska, X. Chen, L. Dai, D. W. K. Ng, and R. Schober. (2017). *Max-min Fair Beamforming for SWIPT Systems With Non-Linear EH Model*. [Online]. Available: https://arxiv.org/abs/1705.05029
[36] Y. Sun, D. W. K. Ng, J. Zhu, and R. Schober, "Multi-objective optimization for robust power efficient and secure full-duplex wireless communication systems," *IEEE Trans. Wireless Commun.*, vol. 15, no. 8, pp. 5511–5526, Aug. 2016.
[37] G. Zheng, K.-K. Wong, and T.-S. Ng, "Robust linear MIMO in the downlink: A worst-case optimization with ellipsoidal uncertainty regions," *EURASIP J. Adv. Signal Process.*, vol. 2008, Jul. 2008, Art. no. 154.
[38] Q. Li and W.-K. Ma, "Spatially selective artificial-noise aided transmit optimization for MISO multi-eves secrecy rate maximization," *IEEE Trans. Signal Process.*, vol. 61, no. 10, pp. 2704–2717, May 2013.
[39] A. Mukherjee and A. L. Swindlehurst, "Detecting passive eavesdroppers in the MIMO wiretap channel," in *Proc. IEEE Intern. Conf. Acoust., Speech Signal Process.*, Mar. 2012, pp. 2809–2812.
[40] S. Zhang, Q. Wu, S. Xu, and G. Y. Li, "Fundamental green tradeoffs: Progresses, challenges, and impacts on 5G networks," *IEEE Commun. Surveys Tuts.*, vol. 19, no. 1, pp. 33–56, 1st Quart., 2017.
[41] Z.-Q. Luo, J. F. Sturm, and S. Zhang, "Multivariate nonnegative quadratic mappings," *SIAM J. Optim.*, vol. 14, no. 4, pp. 1140–1162, 2004.
[42] M. Grant and S. Boyd. (Mar. 2014). *CVX: MATLAB Software for Disciplined Convex Programming, Version 2.1*. [Online]. Available: http://cvxr.com/cvx
[43] J. C. Bezdek and R. J. Hathaway, "Convergence of alternating optimization," *Neural, Parallel Sci. Comput.*, vol. 11, no. 4, pp. 351–368, 2003.
[44] S. Boyd and L. Vandenberghe, *Convex Optimization*. Cambridge, U.K.: Cambridge Univ. Press, 2004.
[45] I. Pólik and T. Terlaky, *Interior Point Methods for Nonlinear Optimization*, G. D. Pillo and F. Schoen, Eds., 1st ed. Berlin, Germany: Springer, 2010.

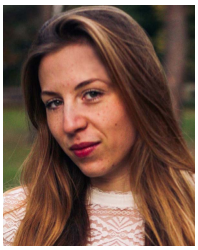

Elena Boshkovska (S'15) was born in Skopje, Macedonia. She received the B.Sc. degree in electrical engineering from Ss. Cyril and Methodius University, Skopje, in 2013, and the M.Sc. degree in communications and multimedia engineering from Friedrich-Alexander-Universität Erlangen-Nürnberg, Germany, in 2015.

Derrick Wing Kwan Ng (S'06–M'12–SM'17) received the bachelor's degree (Hons.) and the M.Phil. degree in electronic engineering from the Hong Kong University of Science and Technology in 2006 and 2008, respectively, and the Ph.D. degree from The University of British Columbia in 2012. From 2011 to 2012, he was a Visiting Scholar with the Centre Tecnològic de Telecomunicacions de Catalunya-Hong Kong. He was a Senior Post-Doctoral Fellow with the Institute for Digital Communications, Friedrich-Alexander-Universität Erlangen-Nürnberg, Germany. He is currently a Senior Lecturer and an ARC DECRA Research Fellow with the University of New South Wales, Sydney, NSW, Australia. His research interests include convex and non-convex optimization, physical layer security, wireless information and power transfer, and green (energy-efficient) wireless communications. He received best paper awards from the IEEE International Conference on Computing, Networking and Communications (ICNC) in 2016, the IEEE Wireless Communications and Networking Conference in 2012, the IEEE Global Telecommunication Conference (Globecom) in 2011, and the IEEE Third International Conference on Communications and Networking in China in 2008. He was honored as an Exemplary Reviewer of the IEEE TRANSACTIONS ON COMMUNICATIONS in 2015, the top Reviewer of the IEEE TRANSACTIONS ON VEHICULAR TECHNOLOGY in 2014 and 2016, and an Exemplary Reviewer of the IEEE WIRELESS COMMUNICATIONS LETTERS in 2012, 2014, and 2015. He has been serving as an Editorial Assistant to the Editor-in-Chief of the IEEE TRANSACTIONS ON COMMUNICATIONS since 2012. He is currently an Editor of the IEEE COMMUNICATIONS LETTERS, the IEEE TRANSACTIONS ON WIRELESS COMMUNICATIONS, and the IEEE TRANSACTIONS ON GREEN COMMUNICATIONS AND NETWORKING.

Linglong Dai (M'11–SM'14) received the B.S. degree from Zhejiang University in 2003, the M.S. degree (Hons.) from the China Academy of Telecommunications Technology in 2006, and the Ph.D. degree (Hons.) from Tsinghua University, Beijing, China, in 2011. From 2011 to 2013, he was a Post-Doctoral Research Fellow with the Department of Electronic Engineering, Tsinghua University, where he was an Assistant Professor from 2013 to 2016. He has been an Associate Professor with Tsinghua University since 2016. He co-authored the book *mmWave Massive MIMO: A Paradigm for 5G* (Elsevier, 2016). He has published over 50 IEEE journal papers and over 40 IEEE conference papers. He also holds 13 granted patents. His current research interests include massive MIMO, millimeter-wave communications, NOMA, sparse signal processing, and machine learning. He has received four conference best paper awards from the the IEEE ICC 2013, the IEEE ICC 2014, the IEEE ICC 2017, and the IEEE VTC 2017. He has also received the Tsinghua University Outstanding Ph.D. Graduate Award in 2011, the Beijing Excellent Doctoral Dissertation Award in 2012, the China National Excellent Doctoral Dissertation Nomination Award in 2013, the URSI Young Scientist Award in 2014, the IEEE TRANSACTIONS ON BROADCASTING Best Paper Award in 2015, the Second Prize of Science and Technology Award of China Institute of Communications in 2016, the IEEE COMMUNICATIONS LETTERS Exemplary Editor Award in 2017, the National Natural Science Foundation of China for Outstanding Young Scholars in 2017, and the IEEE ComSoc Asia-Pacific Outstanding Young Researcher Award in 2017. He currently serves as an Editor of the IEEE TRANSACTIONS ON COMMUNICATIONS, the IEEE TRANSACTIONS ON VEHICULAR TECHNOLOGY, and the IEEE COMMUNICATIONS LETTERS.

Robert Schober (M'01–SM'08–F'10) was born in Neuendettelsau, Germany, in 1971. He received the Diplom degree (Univ.) and Ph.D. degree in electrical engineering from Friedrich-Alexander-Universitäyt Erlangen-Nürnberg (FAU), Germany, in 1997 and 2000, respectively. From 2001 to 2002, he was a Post-Doctoral Fellow with the University of Toronto, Canada, sponsored by the German Academic Exchange Service. From 2002 to 2011, he was a Professor and the Canada Research Chair at The University of British Columbia (UBC), Vancouver, BC, Canada. Since 2012, he has been an Alexander von Humboldt Professor and the Chair for digital communication with FAU. His research interests fall into the broad areas of communication theory, wireless communications, and statistical signal processing.

Dr. Schober is a fellow of the Canadian Academy of Engineering and a fellow of the Engineering Institute of Canada. He is a Member-at-Large of the Board of Governors and a Distinguished Lecturer of the IEEE Communications Society. He received several awards for his work, including the 2002 Heinz Maier-Leibnitz Award of the German Science Foundation, the 2004 Innovations Award of the Vodafone Foundation for Research in Mobile Communications, the 2006 UBC Killam Research Prize, the 2007 Wilhelm Friedrich Bessel Research Award of the Alexander von Humboldt Foundation, the 2008 Charles McDowell Award for Excellence in Research from UBC, the 2011 Alexander von Humboldt Professorship, the 2012 NSERC E.W.R. Stacie Fellowship, and the 2017 Wireless Communications Recognition Award. In addition, he has received several best paper awards for his research. He is currently the Chair of the Steering Committee of the IEEE TRANSACTIONS ON MOLECULAR, BIOLOGICAL AND MULTI-SCALE COMMUNICATION. He is currently serves on the Editorial Board of the PROCEEDINGS OF THE IEEE. From 2012 to 2015, he served as the Editor-in-Chief of the IEEE TRANSACTIONS ON COMMUNICATIONS.